Simultaneous Oxidation/Sulfidation of Cr-Nb Alloys

by

Julia Carmel Duncan

B.S. in Metallurgical Engineering
South Dakota School of Mines and Technology (1985)
B.S. in Chemistry
South Dakota School of Mines and Technology (1987)

Submitted to the Department of Materials Science and Engineering
in Partial Fulfillment of the Requirements for the Degree of

Master of Science
in Materials Science and Engineering

at the

MASSACHUSETTS INSTITUTE OF TECHNOLOGY

MAY 1994

Signature of Author _____
Department of Materials Science and Engineering
May 6, 1994

Certified by _____
Linn W. Hobbs
John F. Elliott Professor of Materials
Thesis Supervisor

Accepted by _____
Carl V. Thompson II
Professor of Electronic Materials
Chair, Departmental Committee on Graduate Students

Science

In memory of Professor Thomas B. King,
who started it all for me at MIT...

Simultaneous Oxidation/Sulfidation of Cr-Nb Alloys

by
Julia Carmel Duncan

Submitted to the Department of Materials Science and Engineering on May 6, 1994 in partial fulfillment of the requirements for the degree of Master of Science in Materials Science and Engineering.

Abstract

A series of alloys containing both Cr and Nb was tested in simultaneous oxidation/sulfidation environments that simulated coal conversion processes, as well as in environments containing only sulfur or oxygen. The sulfur pressures employed ranged from $10^{-7.6}$ to $10^{-4.58}$ atm. Pure oxygen at 1 atm was used as well as gases containing oxygen partial pressures from $10^{-20.6}$ to 10^{-18} atm. All specimens were corroded at either 800°C and 900°C for 20 hours and kinetics were obtained from continuous thermogravimetric measurements. Shorter runs were conducted for examining transient behavior. The samples were analyzed using SEM, environmental SEM with X-ray energy dispersive digital mapping, and glancing angle (0.5°) X-ray diffraction. Corrosion behavior of the alloys was compared to that of pure niobium and pure chromium. Comparisons were made to the kinetic boundary of pure Cr. Gas composition regions that resulted in thin adherent scales were determined. Complex scales were often noted with an oxide and a sulfide. Thin continuous scales of niobium sulfide and chromium oxide were desired to provide maximum protection from further corrosion. A minimum niobium content appeared necessary to activate niobium scale formation and minimum sulfur pressure was necessary to form a continuous niobium sulfide inner layer.

Thesis Supervisor: Linn W. Hobbs
Title: John F. Elliott Professor of Materials

Table of Contents

Abstract **3**
List of Figures **5**
List of Tables **7**
List of Abbreviations Used **8**
Acknowledgments **9**
1.0 Introduction **10**
2.0 Literature Review **11**
3.0 Experimental Procedure **13**
3.1 Alloys and Metals 13
3.2 Specimen Preparation 14
3.3 Isothermal Corrosion Studies 15
3.3.1 Furnace 15
3.3.2 Microbalance 15
3.3.3 SO_2 Runs 17
3.3.4 Gas Mixing 20
3.4 System Calibrations and Checks 21
3.5 Glancing Angle X-Ray Diffraction Analysis 23
3.6 Environmental SEM 24
4.0 Experimental Results **25**
4.1 Oxidation/Sulfidation in SO_2 27
4.1.1 Results at 800°C 27
4.1.2 Results at 1000°C 29
4.2 Sulfidation in H_2-H_2S Mixtures 29
4.2.1 Results at 800°C 29
4.2.2 Results at 900°C 32
4.3 Oxidation/Sulfidation in H_2-H_2O-H_2S Mixtures 41
4.3.1 Results at 800°C 41
4.3.2 Results at 900°C 47
5.0 Discussion **59**
5.1 Oxidation/Sulfidation in SO_2 59
5.2 Sulfidation in H_2-H_2S Mixtures 60
5.3 Oxidation/Sulfidation in H_2-H_2O-H_2S Mixtures 61
5.4 Comparison of CrNb to NbCr 64
5.5 Comparison of Cr-Nb alloys to FeCrNb 64
6.0 Conclusions **66**
7.0 Future Work **67**
8.0 References **70**

List of Figures

3.1 Schematic representation of furnace, microbalance and gas mixing system. 16

4.1 Weight gain versus time for FeCr and CrNb exposed to 1 atm SO_2 at 800°C for 20 hours and CrNb exposed to 1 atm SO_2 at 1000°C. 28

4.2 Weight gain versus time for MA754, Cr, Nb and CrNb exposed to $P_{S_2} = 10^{-6.9}$ atm at 800°C for 20 hours. 30

4.3 ESEM micrographs of CrNb exposed to $P_{S_2} = 10^{-6.9}$ atm at 800°C for 20 hours. 31

4.4 ESEM micrograph of Cr exposed to $P_{S_2} = 10^{-6.9}$ atm at 800°C for 20 hours. 33

4.5 Weight gain versus time for Cr, Nb, CrNb, NbCr and FeCrNb exposed to $P_{S_2} = 10^{-6.9}$ atm at 900°C for 20 hours. 34

4.6 Weight gain versus time for Cr, Nb, CrNb, NbCr and FeCrNb exposed to $P_{S_2} = 10^{-4.6}$ atm at 900°C for 20 hours. 36

4.7 ESEM binary XEDS maps and corresponding micrograph of NbCr exposed to $P_{S_2} = 10^{-6.9}$ atm at 900°C for 20 hours. 37

4.8 ESEM micrograph of CrNb fracture cross section after exposure to $P_{S_2} = 10^{-6.9}$ atm at 900°C for 20 hours. 38

4.9 Weight gain versus time for CrNb exposed to $P_{O_2} = 10^{-4.6}$ atm at 900°C and $P_{S_2} = 10^{-6.9}$ atm at 800°C and 900°C for 20 hours. 39

4.10 Parabolic plot of weight gain versus square root of time for Nb and NbCr exposed to $P_{O_2} = 10^{-4.6}$ atm and $P_{S_2} = 10^{-6.9}$ atm at 800°C for 20 hours. 40

4.11 Weight gain versus time for Cr, Nb and CrNb exposed to $P_{O_2} = 10^{-20.6}$ atm and $P_{S_2} = 10^{-7.6}$ atm at 800°C for 20 hours. 42

4.12 ESEM micrographs of CrNb exposed to $P_{O_2} = 10^{-20.6}$ atm and $P_{S_2} = 10^{-7.9}$ atm at 800°C for 20 hours. 43

4.13 ESEM micrographs of Cr exposed to $P_{O_2} = 10^{-20.6}$ atm and $P_{S_2} = 10^{-7.9}$ atm at 800°C for 20 hours. 44

4.14 ESEM micrograph of Cr exposed to $P_{O_2} = 10^{-20.6}$ atm and $P_{S_2} = 10^{-7.9}$ atm at 800°C for 20 hours. 45

4.15 ESEM micrographs of Nb exposed to $P_{O_2} = 10^{-20.6}$ atm and $P_{S_2} = 10^{-7.9}$ atm at 800°C for 20 hours. 46

List of Figures (continued)

4.16 Weight gain versus time for Cr, Nb and CrNb exposed to $P_{O_2} = 10^{-18}$ atm and $P_{S_2} = 10^{-8}$ atm at 900°C for 20 hours. 48

4.17 ESEM binary XEDS maps of CrNb exposed to $P_{O_2} = 10^{-18}$ atm and $P_{S_2} = 10^{-8}$ a tm at 900°C for 20 hours. 49

4.18 ESEM micrograph of Nb exposed to $P_{O_2} = 10^{-18}$ atm and $P_{S_2} = 10^{-8}$ atm at 900°C for 20 hours. 50

4.19 ESEM binary XEDS maps and corresponding micrograph of CrNb exposed to $P_{O_2} = 10^{-18}$ atm and $P_{S_2} = 10^{-8}$ atm at 900°C for 20 hours. 51

4.20 Weight gain versus time for Cr, Nb, FeCr, FeCrNb, NbCr and CrNb exposed to $P_{O_2} = 10^{-19}$ atm and $P_{S_2} = 10^{-6.5}$ atm at 900°C for 20 hours. 53

4.21 ESEM binary XEDS maps and corresponding micrograph of CrNb fracture cross section exposed to $P_{O_2} = 10^{-19}$ atm and $P_{S_2} = 10^{-6.5}$ atm at 900°C for 20 hours. 55

4.22 ESEM binary XEDS maps and corresponding micrograph of Cr fracture cross section exposed to $P_{O_2} = 10^{-19}$ atm and $P_{S_2} = 10^{-6.5}$ atm at 900°C for 20 hours. 56

4.23 ESEM micrograph of Cr exposed to $P_{O_2} = 10^{-19}$ atm and $P_{S_2} = 10^{-6.5}$ atm at 900°C for 20 hours. 57

4.24 ESEM binary XEDS maps and corresponding micrograph of NbCr fracture cross section exposed to $P_{O_2} = 10^{-19}$ atm and $P_{S_2} = 10^{-6.5}$ atm at 900°C for 20 hours. 58

List of Tables

Table 3.1 Alloys compositions, sources and labels 14

Table 4.1 Summary of alloys and gas mixtures 25

Table 4.2 Summary of gas mixtures 26

Table 4.3 Parabolic or linear reaction rates determined in this study 27

List of Abbreviations Used

(-xx,-xx)	(log oxygen partial pressure, log sulfur partial pressure) in atmospheres for simultaneous oxidation/sulfidation
(-xx)	log partial pressure for either pure oxidation or sulfidation, in atmospheres
atm	atmosphere (pressure)
Cr	99.9995% pure Cr used in this study
CrNb	Cr-40wt%Nb used in this study
EDM	Electrodischarge Machining (also called spark cutting)
ESEM	Environmental Scanning Electron Microscope
FeCr	Fe-45wt%Cr used in this study
FeCrNb	Fe-30wt%Cr-30wt%Nb used in this study
GAXRD	Glancing Angle X-Ray Diffraction
JCPDS	Joint Committee on Powder Diffraction Studies
MA754	Commercial Inconel Mechanical Alloy 754
mg	milligram
ppm	parts per million
Nb	99.998% pure Nb used in this study
NbCr	Nb-45wt%Cr used in this study
RMS	root mean squared
SEM	Scanning Electron Microscope
TGA	Thermogravimetric Analysis; weight gain/time data
WAXS	Wide Angle X-Ray Spectroscopy
XEDS	X-Ray Energy Dispersive Spectroscopy

Acknowledgments

"What happens when you put it all together and it doesn't work?"
"You learn more." - Guenter Arndt

A quick glance at my academic career will attest to how many opportunities I was given to learn. Each can form his own opinion about just how much I assimilated. A partial list of those people who were instrumental during my time here:

Professor M.C. Fuerstenau -- who persuaded me to give MIT a look.
Nancy Fredrickson -- who gave me an excuse to visit MIT, helped me during undergrad and maintained our friendship through all the years.
Professor Julian Szekely -- who saved me from the MIT campus tour and started me thinking about seriously coming here.
Professor Thomas B. King -- whose attitude about research I shall never forget and to whom I will be ever grateful for sharing it with me.
Professor John F. Elliott -- who took me on and taught me valuable lessons.
Professor Linn W. Hobbs -- who took me on despite my history. "Three times a charm." Here's to good wine and my last advisor at MIT. (Knock on wood.)

My former roommates at Ashdown : Aga, Vida, Yoko, Ilana, Cheryl, Ellen, Susan, Lisa, Dan, Ismail, Jim, Erik, William, Evelyn.
Members of my former groups:Edwin, Jackie, Narayan, Andrie, Xuebin, Bob, Charlie, Tim and Matt (JVS' group but close enough).
George Anagnostou for the introduction to Greek cooking and style.

Thanks to:
UROP Bridget Banks for the great year of laughter and help with everything to motors and programming. Brian Gally for help on the EDM and the great chats. Fred Wilson for friendliness and helpfulness when I didn't know who to ask. Joe Adario and Peter Kloumann for X-ray help. Mike Frongillo for tolerance while learning and relearning Electron Microscopy. Dr. Tony Garrett-Reed for help with STEM and aid on the ESEM. Guenter Arndt for help with motors and general confidence building. Bruce A. Pint for advice in the lab, whether I asked for it or not.

My recent research group: Bruce, Chuxin, Sreeram, Lu-Chang, Lara, Effie, Meri
Lara -- I loved rooming with you during the conferences and "squirreling" things away.

Phillippe -- You'll never know just how much of a lifesaver you were.
Ademola Taiwo -- who always put up with me whenever I needed my space and then later wanted someone to talk to.
Waqar Qureshi -- who always made me laugh at MIT or later in letters describing the P-O-R-S-C-H-E. You're right, they all forget about your thesis title or major. I did.
Mark Buonanno --who helped with class work and made me normal at this place. Still going to return the favor and read my Ph.D thesis??
Special thanks to my current housemates Daniel and Lisa Moore for making me feel like family. Here's to the house without J&J!
Christian Honeker -- Vielen Dank! Du hast mir so viel geholfen! Ich kann es kaum zuruckgeben. Jetzt um Beruhmt zu werden und viel Geld zu verdienen! Uns beide.
Ralph Mason -- for giving me something to tease and tolerating me when I did. I'll always remember the Smart Food at generals time.
Martin Romano -- for giving me a life away from MIT.
Beth Stadler -- for making my new office worth the move and without whom I couldn't have gotten this thesis finished, literally. OK, perhaps if we had talked just a little less.. :)

Chapter 1

Introduction

Materials in fossil energy systems are subjected to environments containing both oxygen and sulfur at elevated temperatures. The oxide scales of Cr and Al are commonly utilized in corrosive atmospheres. Unfortunately these materials often catastrophically corrode when exposed to sulfur. Initially protective scales produced by pre-oxidizing eventually breakdown when exposed to sulfur. The refractory metals such as Mo, Ta, W or Nb behave well in sulfidation conditions but have extremely rapid oxidation rates. Materials that exhibit simultaneous oxidation and sulfidation resistance would find considerable utility in several energy applications (such as coal gasification or fluidized bed reactors). Combining an oxidation resistant component (such as Al or Cr) and a sulfidation resistant component (such as Mo, Ta, W or Nb) is one possible way to produce alloy compositions that could be simultaneously resistant. This idea initiated work on the investigation of the simultaneous corrosion resistance of the Cr-Nb binary system. Previous experiments with an Cr-40wt%Nb alloy were performed in pure oxidation and pure sulfidation as well as pre-sulfidation with later oxidation. No exposure to both oxidants had been performed. The aim of this work was to perform these experiments on the alloy. After preliminary results, additional alloys containing chromium or niobium were also included in the study. The corrosion of alloys containing Cr and Nb was studied in sulfidation as well as mixed oxidation conditions at 800°C and 900°C. Experiments were run in pure sulfidation to simulate extreme corrosive environments. In many commercial alloys, the sulfidation poses the limiting factor for use of the material in energy applications.

Chapter 2

Literature Review

Although corrosion studies in mixed oxidants are fairly common, no simultaneous oxidation/sulfidation studies have been conducted on materials containing both Cr and Nb. Limited studies have been made with alloys containing Cr and Nb in oxidizing environments. The work done by Zhou et al. (1991, 1993) on Cr-40wt%Nb was done in either oxidation, sulfidation or a pre-oxidation followed by sulfidation. Sulfidation in 0.76 atm sulfur suggested a formation of protective inner niobium sulfide scale. Chromia was the major product found under oxidation conditions.

Tortorelli and DeVan (1993) conducted oxidation studies on Cr-6a%Nb and Cr-12a%Nb alloys that were also being studied for creep purposes. Their results suggest insufficient Nb content for protection against sulfur in the mixed gases.

Derry and Lees (1976) worked with an Nb-16wt%Cr-4wt%Ni alloy that contained the intermetallic Cr_2Nb and exposed it to air at elevated temperatures. Primarily Nb_2O_5 and $NbCrO_4$ were found at temperatures between 855-1197°C. The exposure times were similar (15 hr vs. 20 hr) to thoseused in this study. Scales would form and detach from the substrate. Several different structures were detailed and activation energies for the formation of each given.

No work to our knowledge has been conducted on binary alloys with two components chosen specifically because one element performed well in oxidation while the other protected in sulfidation conditions. LaBranche (1987) has studied the Cr system extensively and established the existence of a kinetic boundary. A stability diagram employs thermodynamics to delineate regions where sulfides and oxides are expected. The kinetic boundary line distinguishes the area of the stability diagram where nonequilibrium kinetics determine the stable phases.

An entire series of alloys containing Nb in various base metals was investigated in sulfidation by Douglass and coworkers (Chen 1989; Gleeson 1989; Wang 1989) and later in oxidation/sulfidation (He 1992; Kai 1992; Shing 1992). Results were compared to this work.

Work on the sulfidation of niobium has been done by Kofstad (1988), Zhou (1991) and Tatsuki et al (1979). Tatsuki has detailed 10 different niobium sulfides. The sulfidation of refractory metals has been detailed by Strafford and Bird (1979). Douglass et al. (1989, 1992) has done extensive work with a series of alloys containing Nb and the typical base metals (Co, Fe and Ni). With the conditions used (lower sulfur and higher oxygen) the predominant scale was a base-metal sulfide or oxide with no niobium sulfide scale detected. In some cases NbO_2 was observed, which was also sobserved in this study despite gas compositions which fell outside of the NbO_2 stability region.

Superimposing stability diagrams as a method for estimating the behavior of alloys has been used by many researchers in mixed oxidant corrosion. This method was also used by Douglass' research group and specifically for alloys containing Nb (He 1992; Kai 1992; Shing 1992).

Chapter 3

Experimental Procedure

3.1 Alloys and Metals

Table 3.1 shows the compositions and labels for the alloys and metals used in this study. Ames Laboratory, Materials Preparation Laboratory, Ames, Iowa produced several of the alloys in finger-shaped ingots by arc-melting or arc-comelting. The purity of the Cr and Nb used for the Cr-Nb ingots was 99.9995% Iochrome and 99.99% Nb. The appropriate amounts of Nb and Cr were measured into the crucible in the middle of a plate. The system was evacuated and then flushed with ultrahigh purity argon. To further reduce the oxygen content in the chamber, a zirconium button was melted as a gettering agent. When the zirconium button was resolidified and cooled, the arc is started on the ingot materials. The button is allowed to cool, flipped over and remelted a minimum of 6 times to ensure homogeneity. To get the finger-shaped alloy, the button was melted and drawn into the finger mold.

It is common for intermetallic ingots to crack during cooling, due to the brittleness. This resulted in some sections of the ingot containing cracks which were avoided when samples were cut.

Table 3.1 Alloys compositions, sources and labels

Alloy Composition	Made by:	Alloy Label
Cr-40wt%Nb	Ames Lab	CrNb
Nb-45wt%Cr	Ames	NbCr
Fe-30wt%Cr-30wt%Nb	Prof. S. Brown	FeCrNb
Chromium 99.9995%	Ames	Cr
Niobium 99.998	Cabot Co.	Nb
Fe-45wt%Cr	Ames Lab	FeCr
MA754 (Ni-20wt%Cr-0.5wt%Ti-0.3wt%Al-0.05wt%C-0.6vol%Y2O3)	Inconel	MA754

The FeCr is a composition which behaves similarly to pure Cr and is easier to work with; polishing, slicing, and drilling etc. Typical superalloys contain a material such as Fe, Co or Ni as a base material because of its price and workability. Additives are used to improve the corrosion resistance, the machinability, creep properties etc. For this study, a Fe alloy containing Cr and Nb was made to test this theory. Powder metallurgy was used on powders milled to less than 5 μm and then hot isostatically pressed. The resulting alloy was annealed and then sliced using a boron nitride blade. The standard diamond embedded blade on the low speed saw took nearly 4 to 5 times longer to cut.

3.2 Specimen Preparation

- Ingots were sliced into coupons approximately 0.5 to 1 mm with a low speed saw or EDM (for CrNb and NbCr) on a microcurrent setting. A diamond-impregnated blade was used for Cr, Nb, FeCr and a boron nitride blade was utilized for the FeCrNb.
- All samples were polished through 600 grit silicon carbide and then 0.3 mm alumina slurry with water.
- All samples were rinsed just before insertion into the furnace, first with acetone and then with methanol.

3.3 Isothermal Corrosion Studies

A schematic representation of the furnace set-up, the microbalance and the gas mixing system is given in Figure 3.1

3.3.1 Furnace

A vertical tube furnace heated with resistive heating elements was used. High purity alumina was used to avoid evaporation of the refractory and reaction with the oxidants. The diameter of the tube was 3.42 cm for a cross sectional area of 9.18 cm^2. The area was used to calculate the linear flow rate of gases past the sample during an experiment. Platinum gauze was placed at the gas inlet and on a platform directly beneath the hot zone to aid in the equilibration of the gas mixtures. More details are included in the theses of Zhou (1991) and LaBranche (1985), the designer of the set-up.

3.3.2 Microbalance

The strip charts were manually analyzed by drawing a fit through the curve and taking points off the chart. For the first hour, points every 6 minutes were taken (0.1 hr) and then every 12 minutes for the second hour. A point was then taken at 2.5 hours and then every hour after that. This configuration allows for the collection of many data points at the beginning where the weight gain is the most rapid and where the transient behavior is of prime interest.

These points were then plotted with the weight gain normalized by the surface area of the sample (obtained by evaluating the area of the sample silhouette or by using the parameters such as diameter when the sample had a regular shape). Normalized weight gain versus the square root of time was plotted and the data was fit with a square line. The slope of this line was used in figuring out the parabolic rate constant of the weight gain. This could be converted into a rate constant for the overall scale growth by using

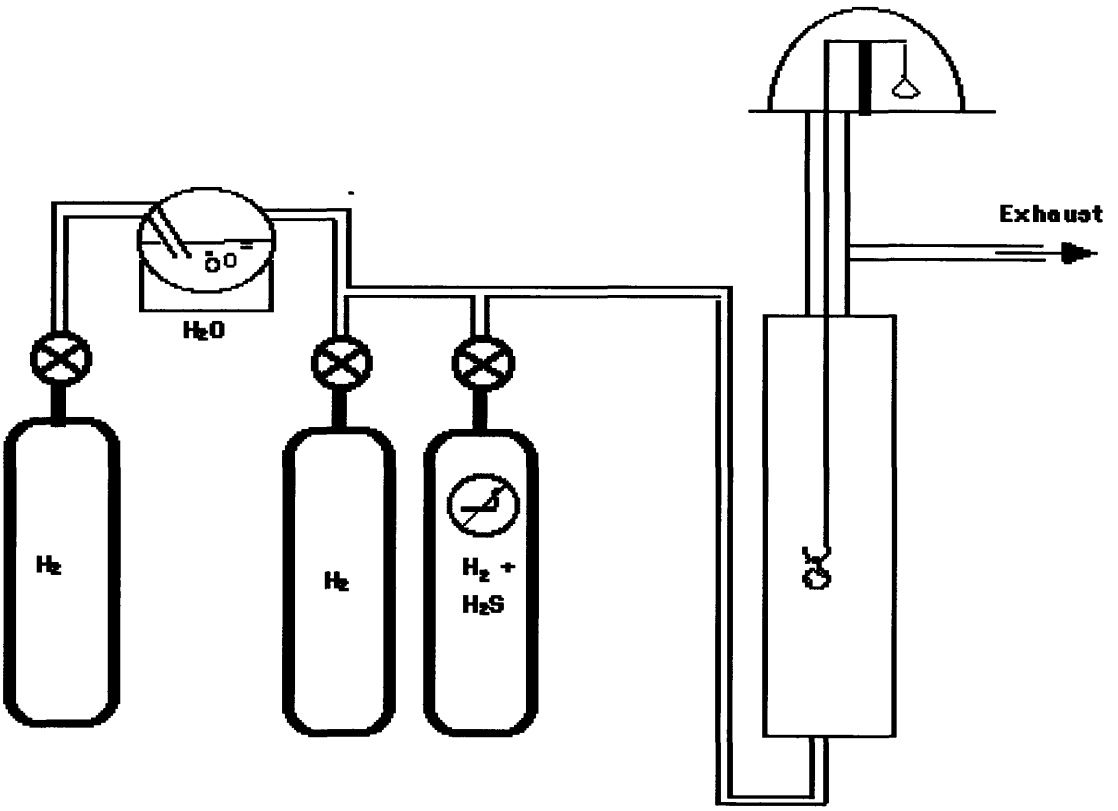

Figure 3.1 Schematic representation of furnace, microbalance and gas mixing system.

the proper stoichiometry of the scale. In many cases, a complex scale precluded such conversion since it would involve estimating thicknesses of each scale component and a more precise determination of the scale. The sulfides produced were often nonstoichiometric and difficult to accurately characterize. Since the comparison of one sample to another was the main goal, such conversion proved unnecessary.

Note that the parabolic rate constants given throughout are the thermogravimetric constants and not corrected to the true parabolic constants. The principal reason for leaving the data in this uncorrected form is the microstructural complexity of the scales result from oxidation/sulfidation experiments. For an accurate conversion to true parabolic rates and diffusion constants, an accurate identification of the scale composition and measurement of the relative amounts of each would be necessary. This amount of precision/detail was not deemed necessary in this study.

3.3.3 SO_2 Runs

Initially, it was hoped that corroding the samples in SO_2 could give a quick estimate of their simultaneous oxidation/sulfidation resistance without the hazard of using H_2S. However, several problems emerged:

- the pressures that resulted are not representative of actual application conditions and difficult to calculate due to multiple equilibria.
- the slightest amount of moisture in the system resulted in the formation of sulfuric acid which condensed on the hangdown chain and gave erroneous weight changes.
- Not only did the sample corrode but the hangdown chain and the terminating sample hook corroded significantly as well.

The relevant chemical equations that describe the equilibrium for SO_2 gas are:

$$\mathbf{SO_2 \rightarrow \tfrac{1}{2}S_2 + O_2} \qquad (1)$$

Any impurity of oxygen, from the gas cylinder or resulting from leaks in the system, as well as oxygen produced from the above equation will provoke the two following equilibria:

$$SO_2 + \frac{1}{2}O_2 \rightarrow SO_3 \qquad (2)$$

$$SO_3 + H_2O \rightarrow H_2SO_4 \qquad (3)$$

Northeast Airgas, supplier of the SO_2 cylinder places the oxygen impurity at less than 500 ppm. This is important in determining the exact oxygen partial pressure. The exact level of oxygen impurity was deemed less important in these studies, since the gas composition is not representative of those used in energy systems; the oxygen partial pressure is significantly higher and the sulfur is towards the lower end of the pressure range typically found in coal systems. Therefore, only a rough indication of simultaneous corrosion resistance could be obtained and the sulfuric acid generation precluded this. The partial pressures of S_2 and O_2 that result from flowing pure SO_2 at 800°C are estimated at $1.3X10^{-8}$ atm and $9.7X10^{-13}$ respectively. These values come from Basu (1989) and assume 50 ppm oxygen impurity in the SO_2. The oxygen and sulfur pressures at 1000°C would be presumably higher, with the negative Gibbs free energy. These were not calculated due to the imprecise knowledge of the O_2 impurity in the tank and the irreproducible SO_2 data .

The second drawback to the SO_2 runs discovered early on is the ease of sulfuric acid formation. Despite many precautions taken to avoid the appearance of water in the system, only a few runs could be conducted before erratic weight gains and losses were registered on the electrobalance. This occurred despite 1) the repeated evacuation of the chamber before the run and refilling with ultrahigh purity argon to displace any water,

2) the purging of argon between runs (sometimes for days to carry any water vapor out through the furnace exit and 3) the drying of the SO_2 gas in a desiccating column before introduction into the furnace. Some of the samples were effectively corroded twice as follows: once via hot corrosion in the furnace and the secondly during the cool down period where the condensation of the acid dripped down the chain and onto the sample. In at least one case, this wet corrosion caused the scale to spall off while in its holder awaiting weighing.

The last drawback to these experiments were the corrosion of the Pt hangdown chain. A blank run of just the hangdown was conducted and the Pt chain gained gained weight in 20 hours. The chain took on a dull grey film or appearance. The Pt-S phase diagram showed a multitude of possible Pt sulfides. The use of the H_2 acts as a reducing agent for the Pt sulfide and prevents its formation in the H_2-H_2O-H_2S mixtures. Since Pt hooks connecting the sample to the hangdown wire were corroded as well, it was difficult to assign the weight gain to the sample or to the corroded Pt hook or Pt hangdown wire. Therefore quartz hangdown hooks, which replaced the lower six inches of the hangdown wire were used to simplify the TGA data analysis. These were easily broken and required the use of a larger hanging hole on the specimen. In addition to fragility, the quartz showed signs of etching and turned a brown-orange color. The maximum use time before replacement was approximately six 20 hour runs.

One advantage with H_2-H_2O-H_2S mixtures is the flexibility and range of gas compositions available. A sample could be exposed to one composition and behave well in terms of corroding slowly with a protective scale and then subjected to more aggressive mixtures (typically less oxygen or more sulfur). In this manner, the point of breakaway corrosion could be pinpointed. The H_2-H_2O-H_2S mixture also allows for

more complete exploration of the stability diagram, where SO_2 basically gives the one ratio of sulfur to oxygen pressure and a small amount of variance by diluting the tank.

3.3.4 Gas Mixing

Gas flow and composition in the furnace was controlled as follows. Constant head manometers (LaBranche 1985) were used to monitor the flow of each individual stream and then the gases were mixed just prior to introduction into the furnace. One gas stream was ultrahigh purity hydrogen which passed through the water to achieve the proper water vapor pressure and a second was a pre-mixed tank of hydrogen and hydrogen sulfide. If necessary, a second diluting line of ultrahigh purity hydrogen could also be used. Argon could also be used for either of the H_2 lines. The proper amounts of each was used using the thermodynamics of the dissolution of both water and hydrogen sulfide into oxygen, hydrogen and sulfur. The relative amounts of gas were chosen using a linear flow rate that was previously determined to be above a diffusion limited reaction (i.e., no boundary layer formed with a local depletion of gas around the sample that would affect the kinetics and alter the actual gas pressures seen by the sample).

The temperature of the presaturator was monitored with an standard laboratory thermometer but the temperature of the circulating bath and therefore the saturator column was measured with a thermometer with $\pm$ 0.1°C accuracy. The controller on the bath itself also controlled the temperature to within 0.1°C of the set temperature.

Heat tape was located on all components and tubing leading up to the furnace that contained water vapor. In addition, heat tape at the exit (the top of the furnace) was wrapped around the glassware (cold zone) to prevent the condensation of either water or sulfur. Water was especially a problem since it could condense on the top portion of the hangdown wire and produce spurious weight gains and losses.

Prior to the starting of a run, the sample was hung and held by a magnet in the cold zone of the furnace. The entire apparatus was sealed off and evacuated using a mechanical pump. Ultrahigh purity argon was introduced at the top (which also protected the microbalance from exposure to any corrosive gases) until ambient conditions were achieved. In cases of extremely low oxygen partial pressures, the chamber was evacuated and filled with ultrahigh purity argon multiple times to eliminate the possibility of residual air contaminating or overwhelming the system. The flows of the gas mixture were allowed into the bottom of the furnace and allowed to flow for at least 30 minutes prior to lowering the sample into the hot zone. The presence of a platinum mesh catalyst a few centimeters below the sample and the initial flushing ensured the equilibration of the gas dissolution and therefore the correct partial pressures as computed. The sample was lowered into the hot zone in fewer than five seconds and kinetic data was simultaneously collected using the Cahn 1000 microbalance.

After the finish of the experiment, typically 20 hours, except for some shorter runs to evaluate initial or transient stages, the sample was quenched from reaction temperature to room temperature within 10 seconds. The gas mixture flow was shut off and the system was purged for a minimum of 30 minutes for safety. As soon as possible after the end of the experiment, the sample was removed and weighed using the Mettler balance to check the thermogravimetric readings.

3.4 System Calibrations and Checks

Flows in the independent manometers were calibrated and verified using a soap bubble and burette. The flow for a specific gas was established and allowed to equilibrate for several minutes. The time for the bubble to sweep a particular volume was measured with a stop watch. This was checked a minimum of three times to ensure a constant flow

rate and was repeated if the flow rate varied. The rates were checked at many points along the flow range and especially at the extreme ends. A plot of the differential of manometer heights and flow rates was plotted and points were repeated if a straight line fit to the data had a root mean square (RMS) of less than 0.95. Often the RMS was 1.00 or very close. This was done for each gas run though each manometer and each capillary in the manometer. The straight line fit was used later in the computer program to calculate the delta height in the manometer necessary to achieve the proper flow. Periodically these points would be checked again to verify their accuracy.

To ensure equilibrium water saturation, a presaturator was used that was set a minimum of 10°C higher than the calculated water saturator temperature. This equilibrium was also checked to ensure that a flow rate was not used that was too high or too fast to allow for the gas to pick up the equilibrium amount of water vapor. Vapor pressures on the high range of those required for the experiments (and therefore saturator temperatures on the high range of those used) were also tested to see if these could also achieve equilibrium. The gas was allowed to flow through a glass tube with several holes in it (which eliminates back pressure) in contrast to a frit which would finely divide the gas into bubbles and increase the surface area and allow for more equilibrium water vapor pickup but possible restrict the gas flow.

The vapor-saturated gas (typically hydrogen, though argon was also used) was passed through a U-tube with P_2O_5 to verify equilibrium water pressure. The U-tube was weighed before and after with the Mettler balance (with 4 decimal point accuracy). The gas was started through the saturator and allowed to flow at least 5-10 minutes to achieve equilibrium. The flow was then shunted through the U-tube and accurately timed (typically 30 minutes) to obtain a good average and also to pick up enough water to be accurately measured. An error of less than 8% was found in every case, including both

extremes in the saturator temperature and in the high flow rates. Errors could be attributed to the condensation of water immediately before or after the U-tube. Heat tape was used on all portions of tubing containing water in the flow, but the presence of silicon rubber as connections in the U-tube set-up precluded using heat tape on every part of the system. This caused some condensation right before the U-tube and the U-tube inlet valve. Indeed, some condensation was visible which was exposed to the ambient environment and evaporated before weighing was completed.

A final check on the system, to verify that the gas pressures achieved were the actual calculated ones, was a reproduction of the kinetic boundary experiments for pure chromium as done by LaBranche (1987). Verification was done at 900°C for 20 hours. The gas mixture D (-18.0, -6.6) lies within the oxide stability regime and Cr exposed to this composition grew a chromia scale with very nearly the same weight gain as that found by LaBranche (1987) (0.5 mg/cm^2 versus 0.4 mg/cm^2 found in this study). The gas mixture labeled C (-18.0, -5.6) is situated within the experimentally determined sulfide region of the kinetic boundary; Cr exposed to this composition formed a rapidly growing, thick sulfide scale. Similar to results by LaBranche, the sulfide weight gains were not reproducible as chromia scale weight gains, but lay within the same large range.

3.5 Glancing Angle X-Ray Diffraction Analysis

Glancing angle X-ray diffraction was conducted using the Rigaku 200 scanning diffractometer. Typically theta was fixed at 0.5° and two theta was scanned from 20° to 139°. The typical voltage used was 50 KV and 150 mA although some diffraction spectra were taken at 60 KV and 180 mA to increase the amount of signal. A scattering/diffracting slit of 0.2 was used. No height limiting slits were used. Spectra were kept to the same parameters so as to overlay two scans and to compare the scales of one sample to another. GAXRD proved useful for shallow penetration and for obtaining signal from the thin film or scale only and not the substrate, thus avoiding extra peaks

that would have obscured the characterization. Due to the overlap of many peaks, especially when dealing with sulfides, often the comparison was the most useful.

3.6 Environmental SEM

The samples surfaces and cross sections were examined primarily in the environmental SEM, which allowed imaging without coating the sample which may have altered the structure. The absence of coating also allowed for further analyses without concern for sample contamination from the evaporated coating. (e.g. GAXRD).

The ESEM produced binary XEDS maps of cross sections, particularly those obtained by fracture. Fracture cross section allowed observation of grain structure and reduced sample contamination due to polishing. The slightly irregular surface improved image contrast; the smooth polished surface proved difficult to focus on. Highly irregular surfaces created artifacts due to the highly sensitive specimen to detector distance and configuration of the detector relative to the sample. The X-ray detector was located 2° below the sample holder and required the tilting of the sample (approximately 20-25°) to allow emitted X-rays to reach the detector.

Chapter 4

Experimental Results

An overview of all corrosion experiments is given in Table 4.1. Gas mixtures employed in this study and their labels are shown in Table 4.2. Table 4.3 gives the parabolic and linear corrosion rates found in this study. As noted in the List of Abbreviations, pressures are given in atmospheres in the format: (log P_{O_2}, log P_{S_2}) or simply (log P_{X_2}) for corrosion in a single oxidant.

Table 4.1 Summary of alloys and gas mixtures

Alloy Label	SO_2		H_2-H_2S		H_2-H_2O-H_2S	
	800°C	1000	800	900	800	900
CrNb	X	X	X	X	X	X
NbCr				X		X
FeCrNb				X		X
Cr			X	X	X	X
Nb	X		X	X	X	X
FeCr	X	X			X	X
MA754	X					

Table 4.2 Summary of gas mixtures

Gas Composition Label	**P_{O_2} (log P_{O_2}) in atm**	**P_{S_2}(log P_{S_2}) in atm**
SO_2	$9.7X10^{-13}$ * (-12.1)	$1.3X10^{-8}$* (-7.9)
A	$2.8X10^{-21}$ (-20.6)	$2.4X10^{-8}$ (-7.6)
B	$1.0X10^{-18}$ (-18.0)	$1.0X10^{-8}$ (-8.0)
C	$1.0X10^{-18}$ (-18.0)	$2.5X10^{-6}$ (-5.6)
D	$1.0X10^{-18}$ (-18.0)	$2.5X10^{-7}$ (-6.6)
E	$2.5X10^{-20}$ (-19.6)	$2.8X10^{-8}$ (-7.6)
F	$1.0X10^{-19}$ (-19.0)	$3.2X10^{-7}$ (-6.5)
Ox	1.0 pure oxygen	- -
X	$1.0X10^{-}18$ (-18.0)	- -
S1	- -	$1.1X10^{-7}$ (-6.9)
S2	- -	$2.7X10^{-5}$ (-4.6)
* assuming 50 ppm oxygen impurity in the cylinder		

Table 4.3 Parabolic or linear reaction rates determined in this study.

	Parabolic rates in units of g^2/cm^4 s *Linear rates in units of g/cm^2 s*					
Gas Mix/Temp	Cr	Nb	CrNb	NbCr	FeCr	FeCrNb
SO_2 800°C			1.8×10^{-11}			
A 800°C	1.8×10^{-8}	2.5×10^{-11}	1.0×10^{-9}		1.5×10^{-7}	
B 900°C	2.0×10^{-12}	*1.0×10^{-7}*	1.0×10^{-11}			
C 900°C	1.0×10^{-7}		*5.3×10^{-7}*			
D 900°C	1.3×10^{-12}					
E 800°C		1.6×10^{-11}				
F 900°C			7.6×10^{-12}	2.0×10^{-11}	8.3×10^{-11}	1.2×10^{-10}
S1 800°C	*2.0×10^{-6}*	3.5×10^{-12}	1.0×10^{-8}			
S1 900°C	*1.3×10^{-6}*	4.0×10^{-13}	1.5×10^{-8}	2.5×10^{-11}		*8.8×10^{-7}*
S2 900°C			4.7×10^{-8}	7.5×10^{-11}		1.0×10^{-7}

4.1 Oxidation/Sulfidation in SO_2

Simultaneous oxidation/sulfidation was studied by exposing the alloys to pure SO_2 gas.

4.1.1 Results at 800°C

Pure Nb, FeCr, CrNb and MA754 (NiCrAl) were corroded in pure SO_2. Condensation on the hangdown wire occurred for many samples. The erratic weight gains yielded little useful kinetic data. Figure 4.1 displays weight gains for experiments with uncompromised TGA data. Parabolic rate constants for the CrNb and the FeCr were both of order $1X10^{-11}$ g^2/cm^4 sec. The Nb samples exhibited breakaway corrosion with linear weight gains and frequently fell off at temperature before 10 hours. The samples which remained on the hangdown hook at temperature for 3.2 and 4.6 hours cracked and

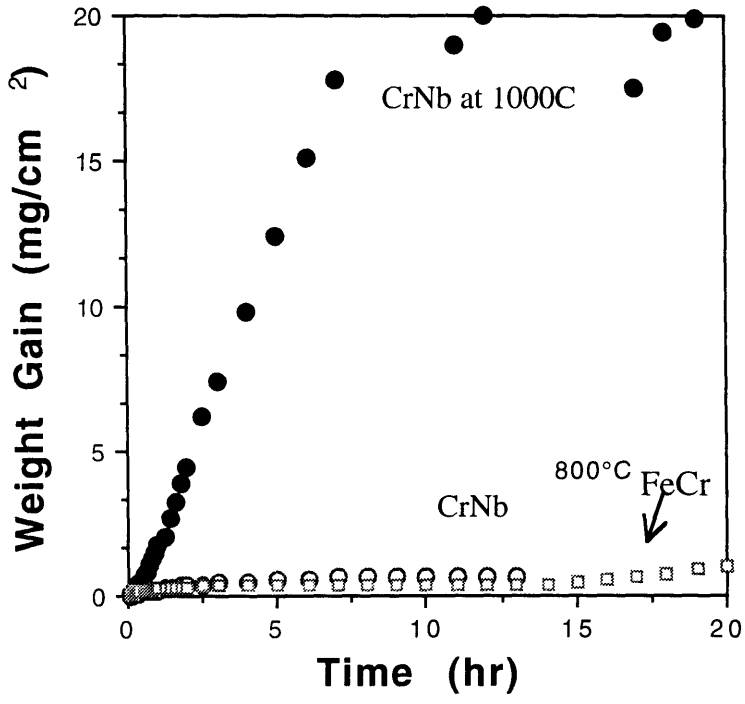

Figure 4.1 Weight gain versus time for FeCr and CrNb exposed to 1 atm SO_2 at 800°C for 20 hours and CrNb exposed to 1 atm SO_2 at 1000°C.

fell off while cooling to room temperature in the cold zone. MA754 runs gave no reproducible kinetic data and the removed samples were coated with a caustic black liquid.

4.1.2 Results at 1000°C

Only CrNb and FeCr were run in SO_2 at this temperature. The CrNb exhibited a linear corrosion rate of $7X10^{-7}$ g/cm^2 sec and the sample was coated with black liquid upon removal. The corroded FeCr samples were wet upon removal and the TGA data were not analyzed because of the numerous jumps in the weight gain curves. The wet scale spalled on cooling.

4.2 Sulfidation in H_2-H_2S Mixtures

Pure sulfidation experiments were conducted to simulate extreme corrosive environments. In many commercial alloys, sulfidation represents the extreme condition for use of the material in energy applications.

4.2.1 Results at 800°C

Pure sulfidation experiments were conducted at $P_{S_2} = 1.1X10^{-7}$ atm (Composition S1) in flowing gas from a pre-mixed tank of H_2-2.23vol%H_2S. Figure 4.2 shows the TGA data at this gas composition. The CrNb weight gain was intermediate between its pure constituents. The adherent scale exhibited a shine and macroscopic facets (Figure 4.3). GAXRD measurements showed a mix of chromium sulfides; overlap of peaks made it difficult to resolve into specific sulfides. Either Cr_2S_3 or Cr_3S_4 or a mixture of both are possible scale compositions. A fracture cross section indicated columnar grains and a niobium rich region at the scale/metal interface. The latter may indicate a niobium sulfide inner scale. GAXRD data were unable to confirm this.

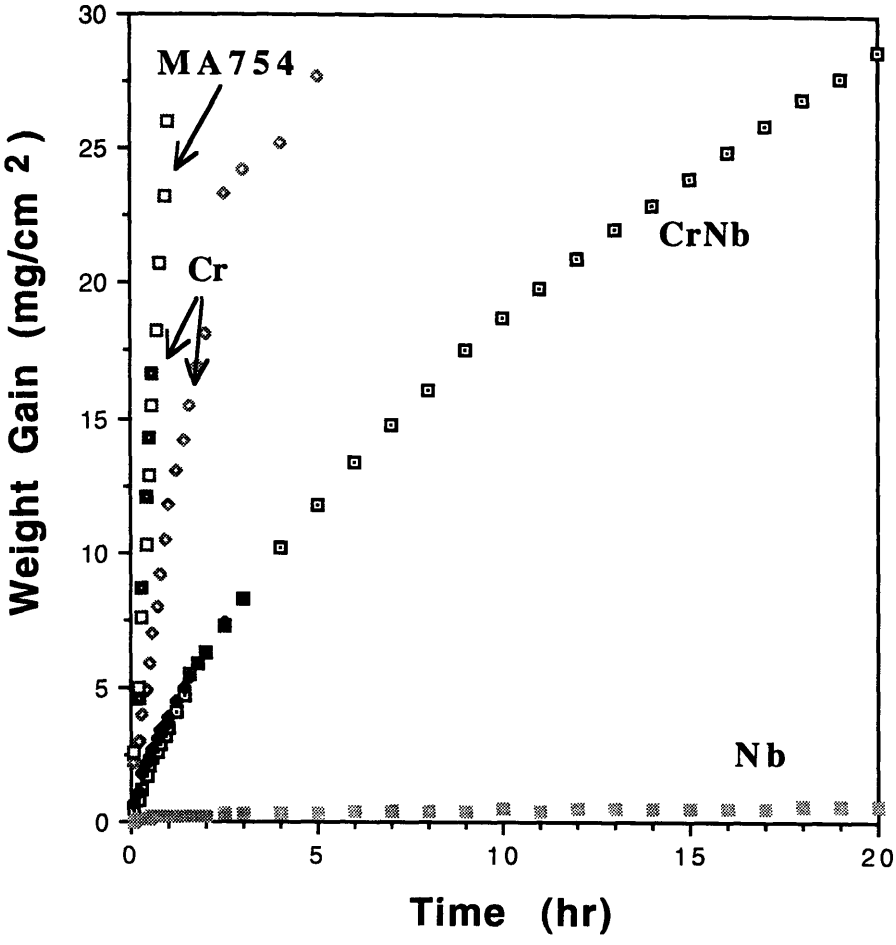

Figure 4.2 Weight gain versus time for MA754, Cr, Nb and CrNb exposed to $P_{S_2} = 10^{-6.9}$ atm at 800°C for 20 hours.

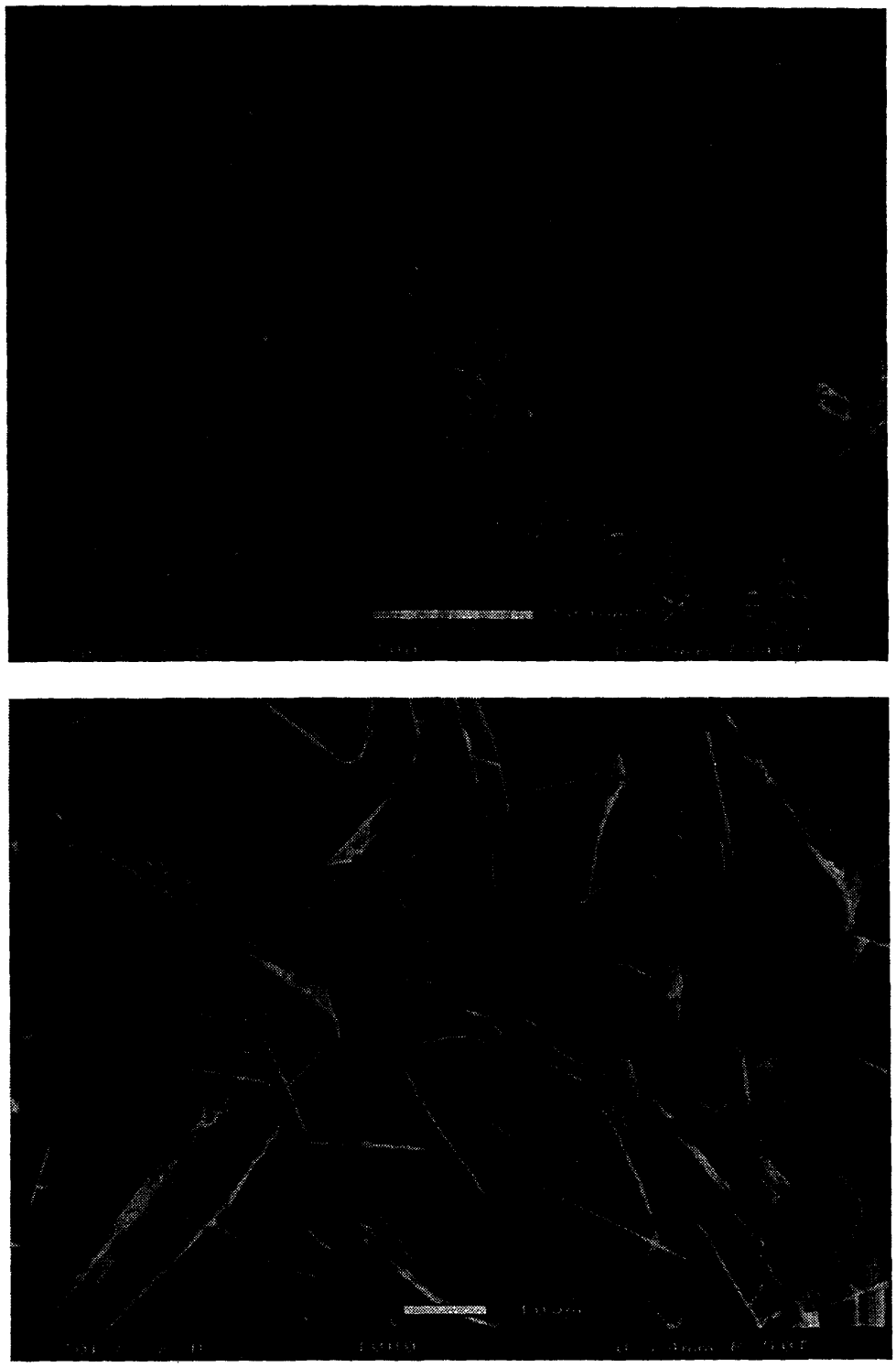

Figure 4.3 ESEM micrographs of CrNb exposed to $P=10^{-6.9}$ atm at 800°C for 20 hours.

The sulfidation rate of Cr was linear after 3 hours; Figure 4.4 shows the sulfide scale. Nb sulfidized in a slow, parabolic manner to $Nb_{(1-x)}S$. The Nb appeared barely tarnished, with a dark, uniform appearance and a very small weight gain on the order of the typical balance drift and fluctuations. The MA754 exhibited linear corrosion rates on the same order as for Cr. Balls of scale formed on the surface of the sample; the melting point for nickel sulfide is 799°C, so the reaction product was presumably liquid and was "dripping" off the sample at temperature.

4.2.2 Results at 900°C

Sulfidation in gas composition S1 was also conducted at 900°C; the results are given in Figure 4.5. The weight gains were parabolic for CrNb, NbCr and Nb and linear for FeCrNb and Cr. CrNb and NbCr had weight gains intermediate between Cr and Nb. The Nb weight gains were so low that accurate values could not be determined. Various sections on the Nb curve could be interpreted as parabolic with parabolic rates that ranged from 10^{-12} to 10^{-13} g^2/cm^4 sec while NbCr yielded a parabolic rate of 10^{-11} g^2/cm^4 sec. The scales on Cr and CrNb exhibited metallic shine; spallation was observed at the edges of the CrNb and the NbCr samples. GAXRD analysis on both surfaces of the spalled NbCr scale, as well as on the surface exposed under the spall, was conducted. Scans of both sides of the spalled scale showed no significant difference in the X-ray diffraction spectra. However, there was a notable difference in the scans of the spalled material and the substrate beneath it. Significantly, the niobium sulfide peak was stronger under the spalled scale. An incubation period of low weight gain was observed for FeCrNb before large weight gains commenced. The scale was also faceted with its edges spalling. GAXRD from the scales of CrNb and NbCr indicated an outer chromium sulfide and an inner niobium sulfide. Cr_2S_3 was evident for both alloys but the niobium sulfide phase differed: NbS_2 for the NbCr and $Nb_{(1-x)}S$ in the CrNb scale. The scale on FeCrNb contained Cr_2S_3 in addition to $Fe_{(1-x)}S$. The scale on Cr was either Cr_2S_3 or Cr_3S_4, while the Nb sulfidized to a combination of NbS_2 and Nb_3S_4.

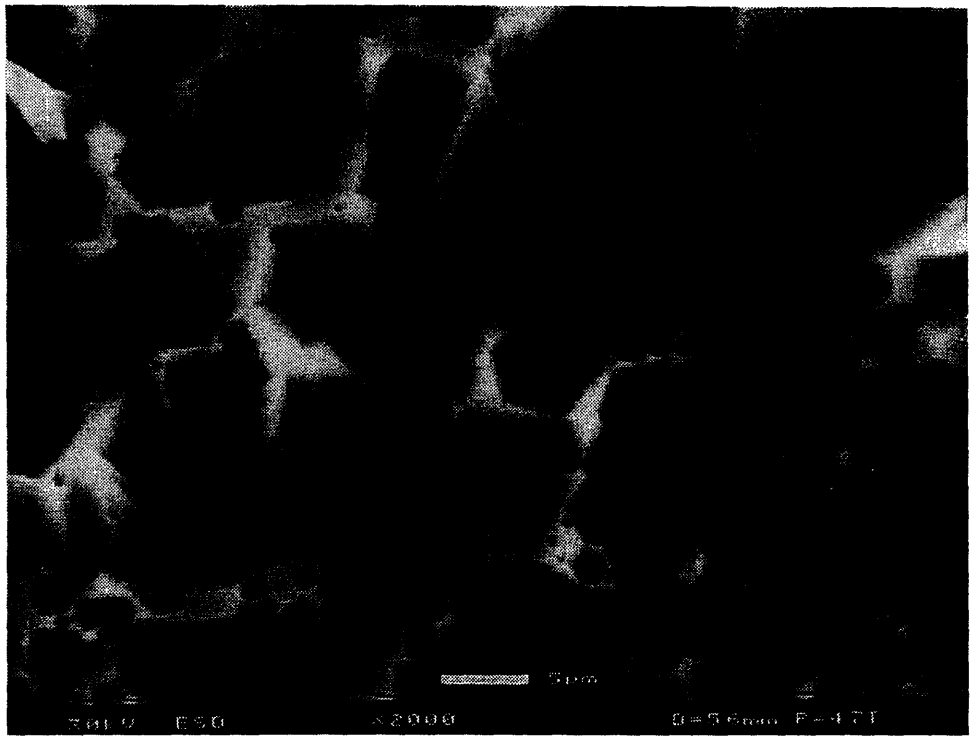

Figure 4.4 ESEM micrograph of Cr exposed to $P_{S_2} = 10^{-6.9}$ atm at 800°C for 20 hours.

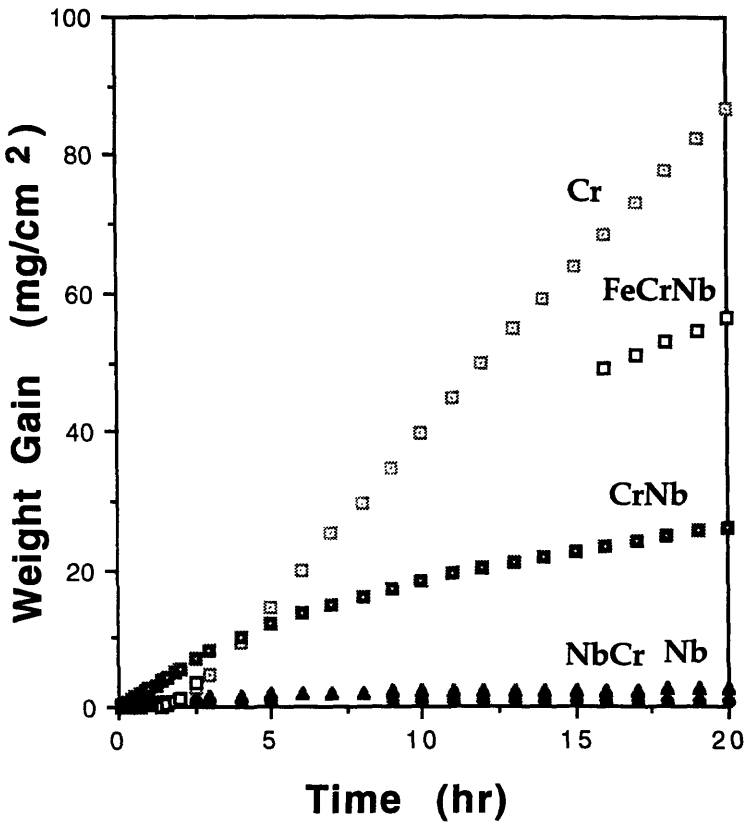

Figure 4.5 Weight gain versus time for Cr, Nb, CrNb, NbCr and FeCrNb exposed to P_{S_2} = $10^{-6.9}$ atm at 900°C for 20 hours.

S2 at 900°C Pure sulfidation was also conducted at a higher sulfur pressure of $P_{S_2} = 2.65X10^{-5}$ atm (S2) at 900°C. A weight gain comparison of the alloys exposed to this composition is shown in Figure 4.6. Again, the two alloys had gains intermediate of those of the pure constituents and, again, the rate of NbCr very nearly matched the rate of pure niobium. The NbCr scale was adherent, as were the other scales. The parabolic rate for NbCr was orders of magnitude smaller than for CrNb (10^{-10} versus 10^{-8} g^2/cm^4 sec), though GAXRD and ESEM XEDS indicated a Cr_2S_3 scale and an NbS_2 inner scale for both. Figure 4.7 presents a fracture cross section and digital maps of the scale for NbCr in S2, while Figure 4.8 shows a CrNb fracture cross section.

Since the sulfur pressure influenced the adhesion of the NbCr scale, an experiment was conducted where the sulfur pressure was altered at temperature. After 2 hours of S1 exposure, the gas mixture was switched to S2, which had produced an adherent scale in the isothermal 20 hr experiment. The resulting scale was adherent, and the corrosion rate was noticeably altered after the gas composition switch.

Kinetics for pure sulfidation of the CrNb alone at two different sulfur partial pressures and two different temperatures are shown in Figure 4.9. In composition S1, there was little effect of temperature seen. The alloy was exposed to composition S2 at 900°C and exhibited a parabolic rate approximately three times higher than the rate in atmosphere S1 at 900°C.

The effect of the sulfur partial pressure for NbCr and Nb at 900°C is shown in Figure 4.10. The rates were within one order of magnitude of each other, approximately 10^{-10} g^2/cm^4 sec, independent of the pressure. One notable difference was the lack of spallation at the higher sulfur pressures. The curves showed parabolic behavior within different regimes.

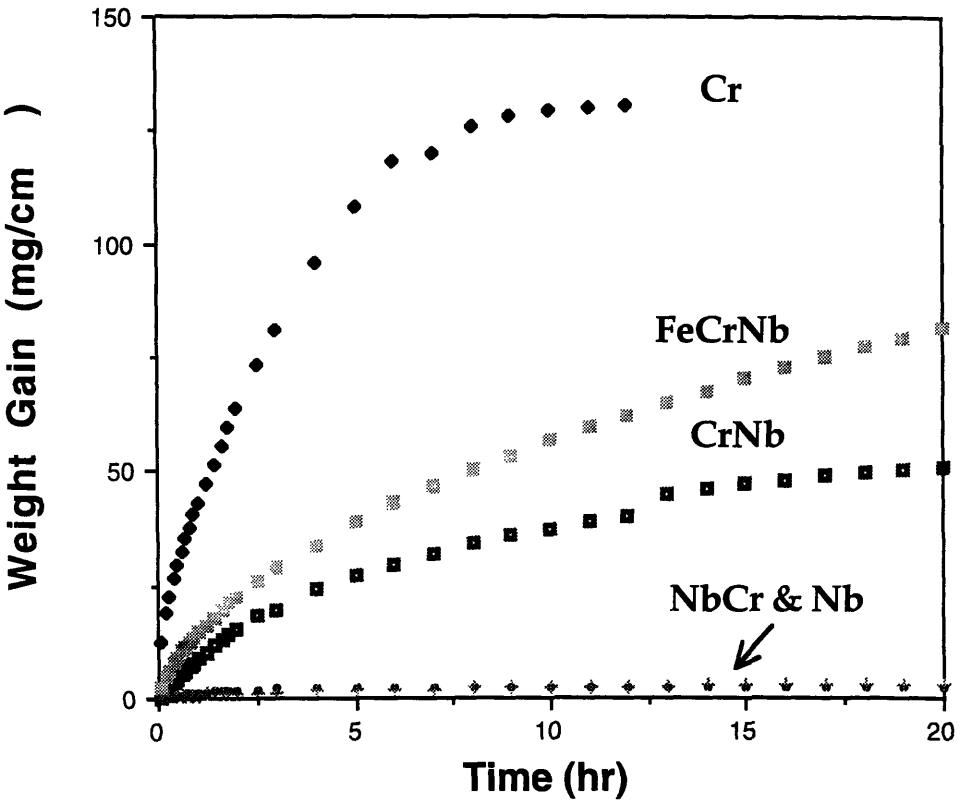

Figure 4.6 Weight gain versus time for Cr, Nb, CrNb, NbCr and FeCrNb exposed to P_{S_2} = $10^{-4.6}$ atm at 900°C for 20 hours.

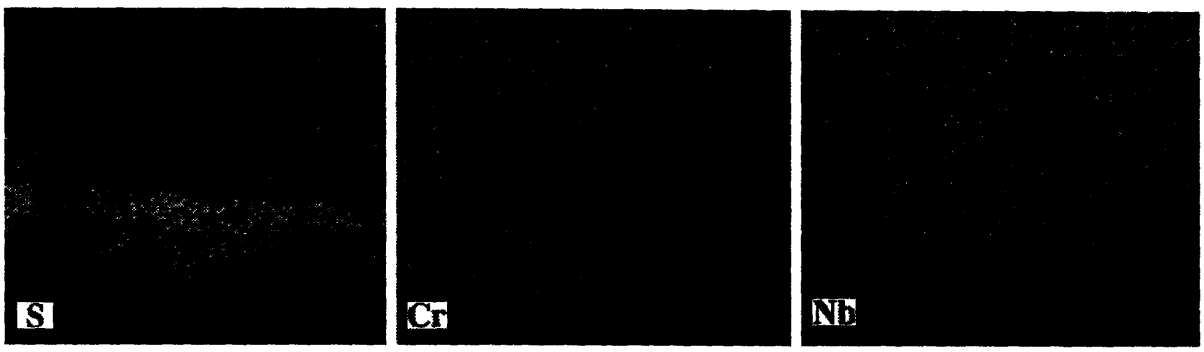

a)

b)

Figure 4.7 ESEM binary XEDS maps and corresponding micrograph of NbCr exposed to $P_{S2} = 10^{-6.9}$ atm at 900°C for 20 hours.

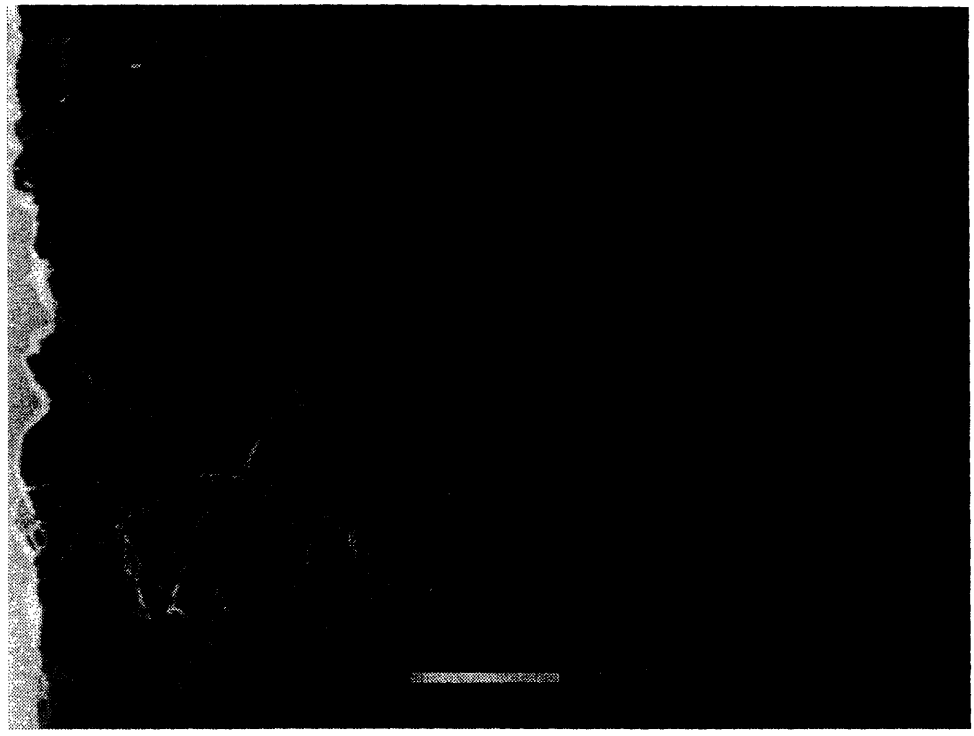

Figure 4.8 ESEM micrograph of a CrNb fracture cross section after exposure to $P_{S_2} = 10^{-4.6}$ atm at 900°C for 20 hours.

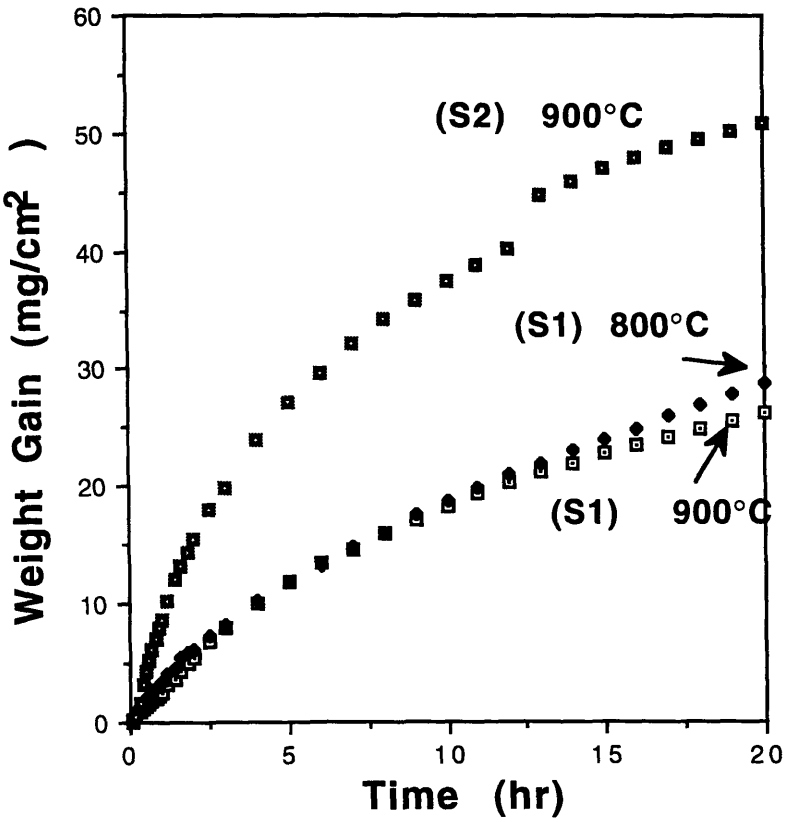

Figure 4.9 Weight gain versus time for CrNb exposed to $P_{S_2} = 10^{-4.6}$ atm at 900°C and $P_{S_2} = 10^{-6.9}$ atm at 800°C and 900°C for 20 hours.

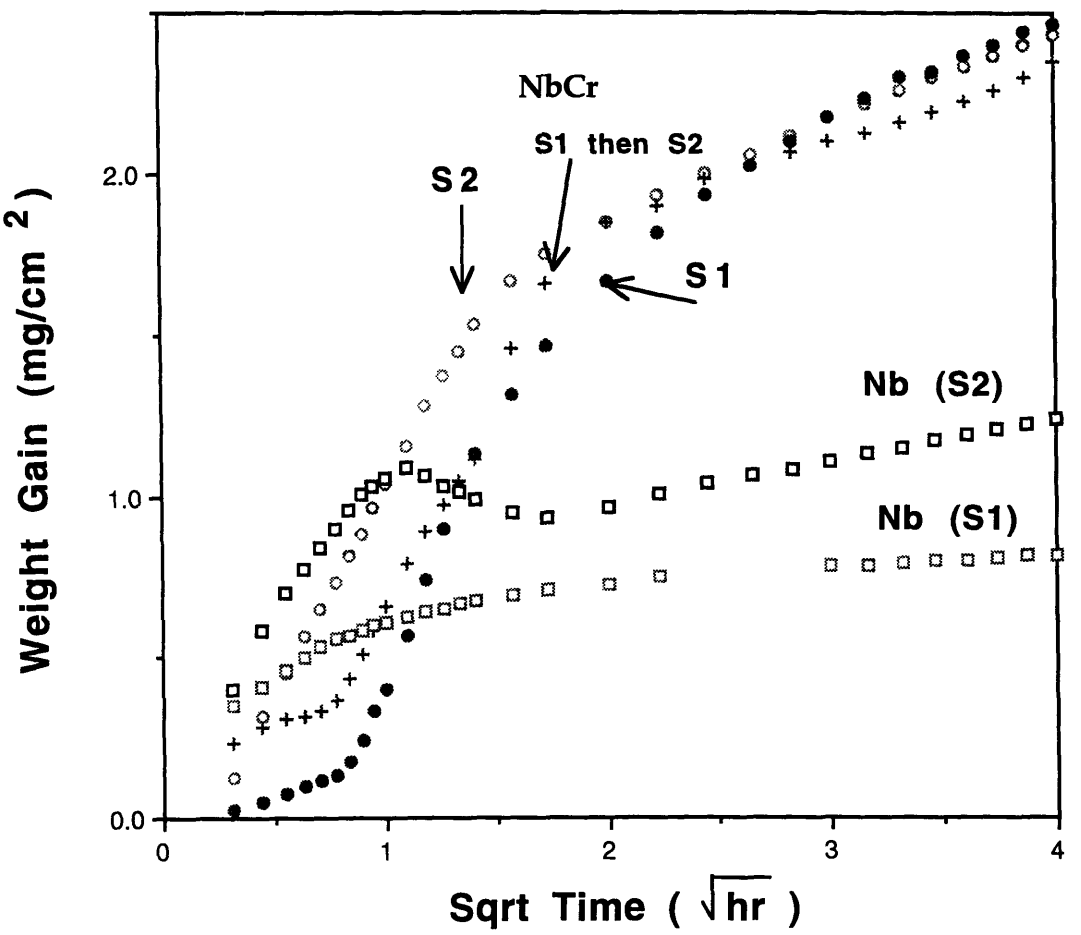

Figure 4.10 Parabolic plot of weight gain versus square root of time for Nb and NbCr exposed to $P_{S_2} = 10^{-4.6}$ atm and $P_{S_2} = 10^{-6.9}$ atm at 800°C for 20 hours.

There was also a significant difference in the scale composition of the NbCr in S1 as opposed to the S2 gas composition. Kinetics were not appreciably different but X-ray scans indicated different sulfides phased formed.

4.3 Oxidation/Sulfidation in H_2-H_2O-H_2S Mixtures

Three main compositions (A, B and F) were used to study simultaneous oxidation/sulfidation. Additional mixtures were used to evaluate the effect of varying composition for certain experiments.

4.3.1 Results at 800°C

Simultaneous oxidation/sulfidation was conducted at 800°C with gas composition A. TGA results are shown in Figure 4.11. The CrNb exhibited a parabolic rate intermediate between the pure components. GAXRD showed the scale composition to be a mix of chromia and chromium sulfides. Macroscopically, the scale was dark with silvery patches which may have undergone spallation (Figure 4.12). The scale on Cr was also a mix of oxide and sulfides with macroscopic surface roughness in the shape of blades or large needles (Figures 4.13 and 4.14). The scale on the niobium, which was the slowest growing, consisted of NbO_2. SEM examination showed a dense scale, with no spallation but some evidence of cracks; small particles of Nb_2O_5 were evident on top of the scale (Figure 4.15).

Gas Composition E (-19.6, -7.6) A gas composition one order of magnitude higher in oxygen pressure was used to observe the scale composition of Nb and note if Nb_2O_5 was formed. After 20 hours, the scale showed no difference from the scale formed in gas A. GAXRD again showed NbO_2 as the primary scale product, with very minor differences in the diffraction spectra.

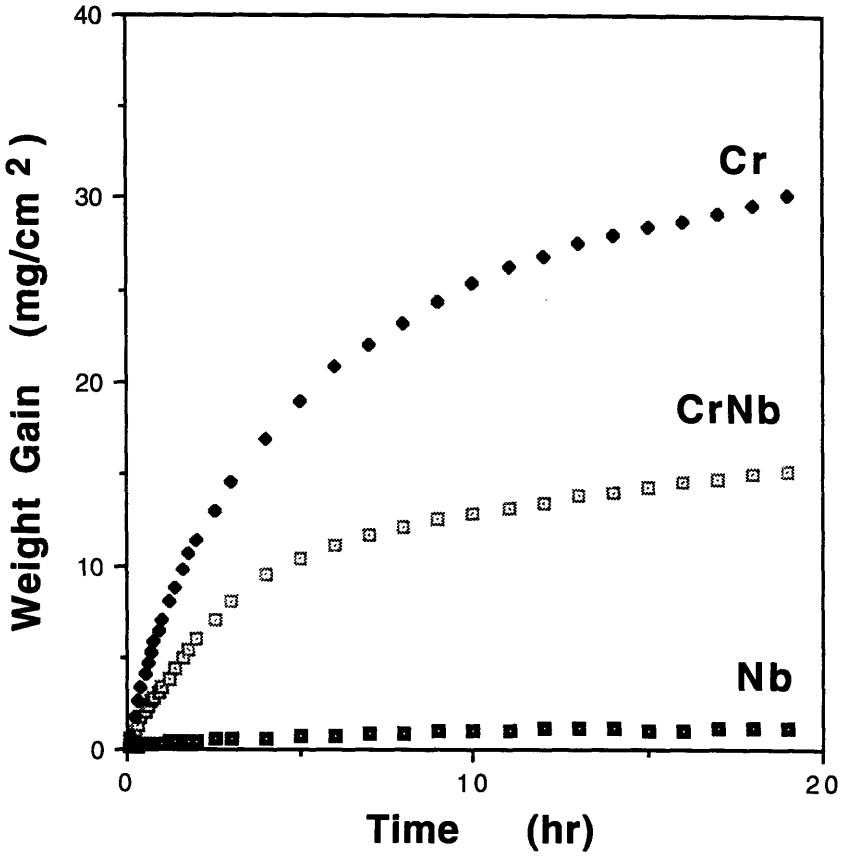

Figure 4.11 Weight gain versus time for Cr, Nb and CrNb exposed to $P_{O_2} = 10^{-20.6}$ atm and $P_{S_2} = 10^{-7.6}$ atm at 800°C for 20 hours.

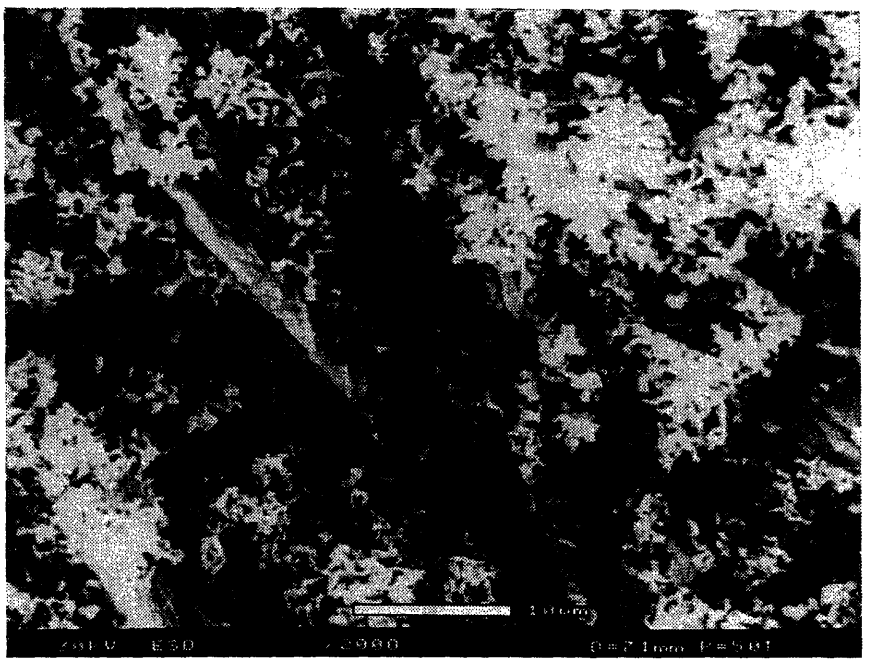

a)

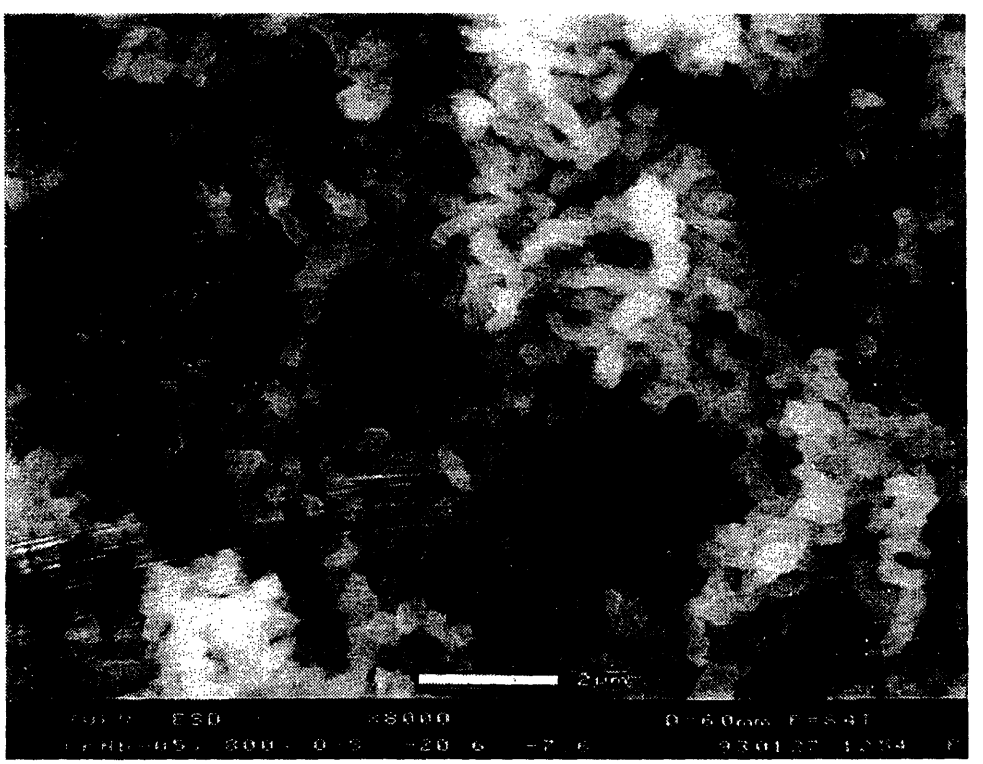

b)

Figure 4.12 ESEM micrographs of CrNb exposed to $P_{O_2} = 10^{-20.6}$ atm and $P_{S_2} = 10^{-7.9}$ atm at 800°C for 20 hours: (a) sulfide with overlying chromia, and (b) magnified image of chromia overlayer.

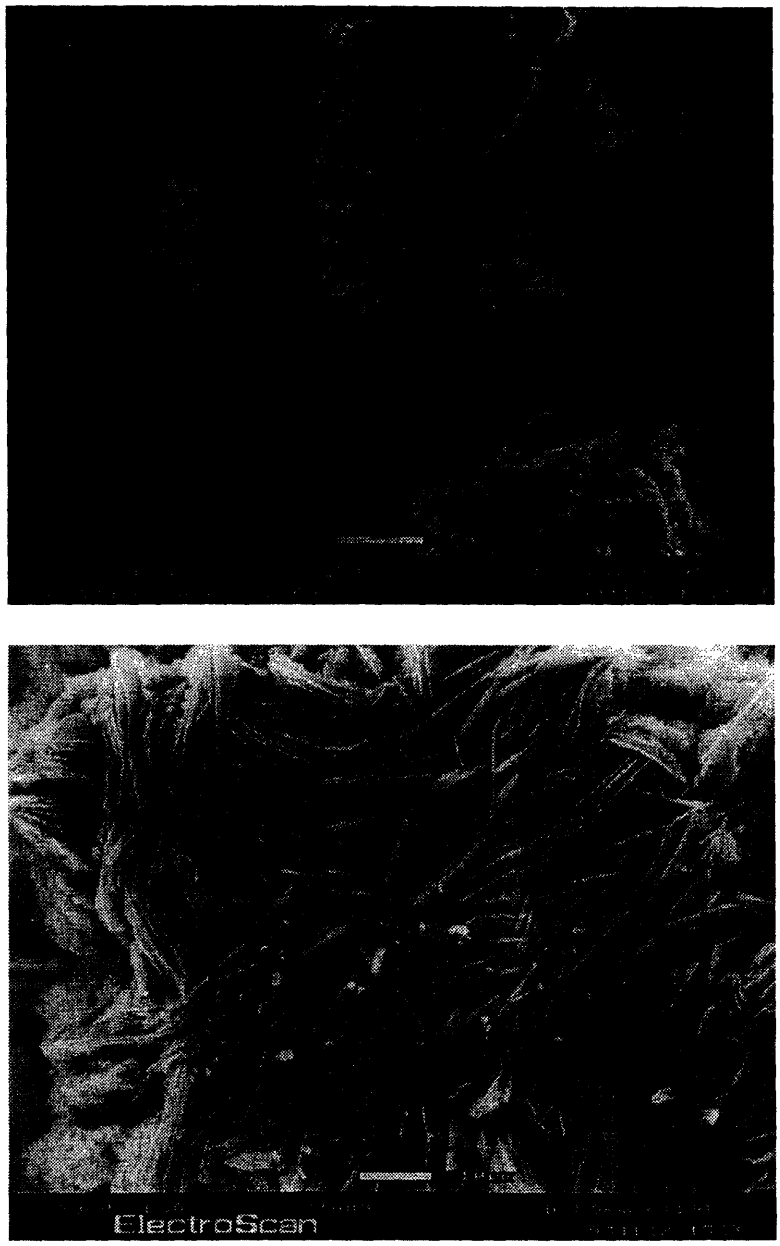

Figure 4.13 ESEM micrographs of Cr exposed to $P_{O_2} = 10^{-20.6}$ atm and $P_{S_2} = 10^{-7.6}$ atm at 800°C for 20 hours.

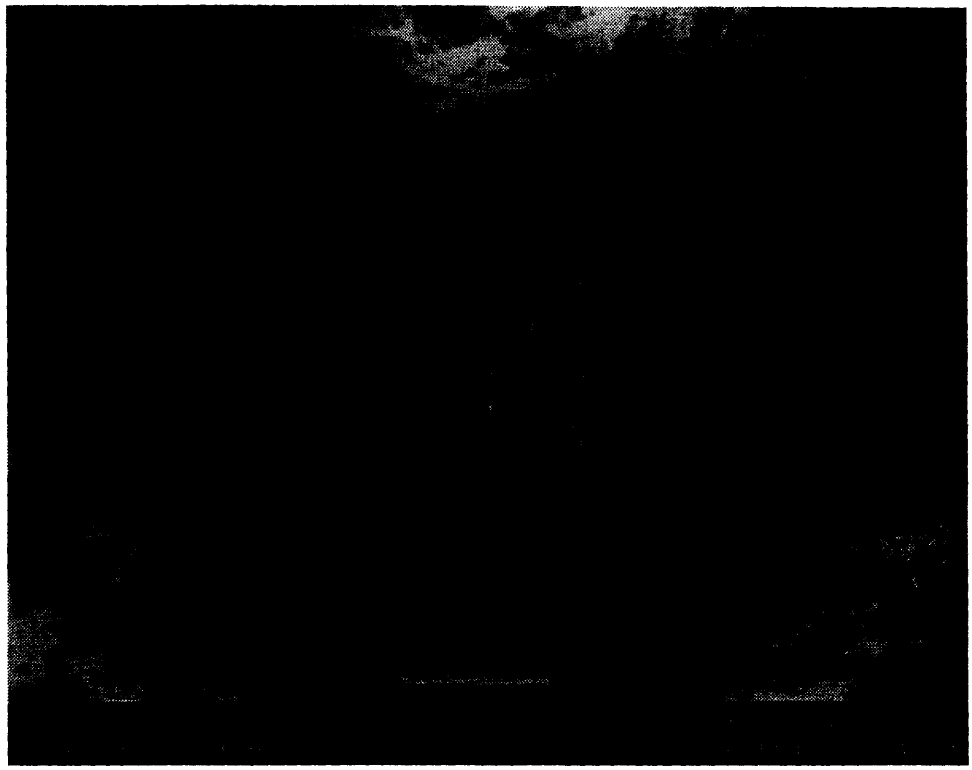

Figure 4.14 ESEM micrograph of Cr exposed to $P_{O_2} = 10^{-20.6}$ atm and $P_{S_2} = 10^{-7.6}$ atm at 800°C for 20 hours.

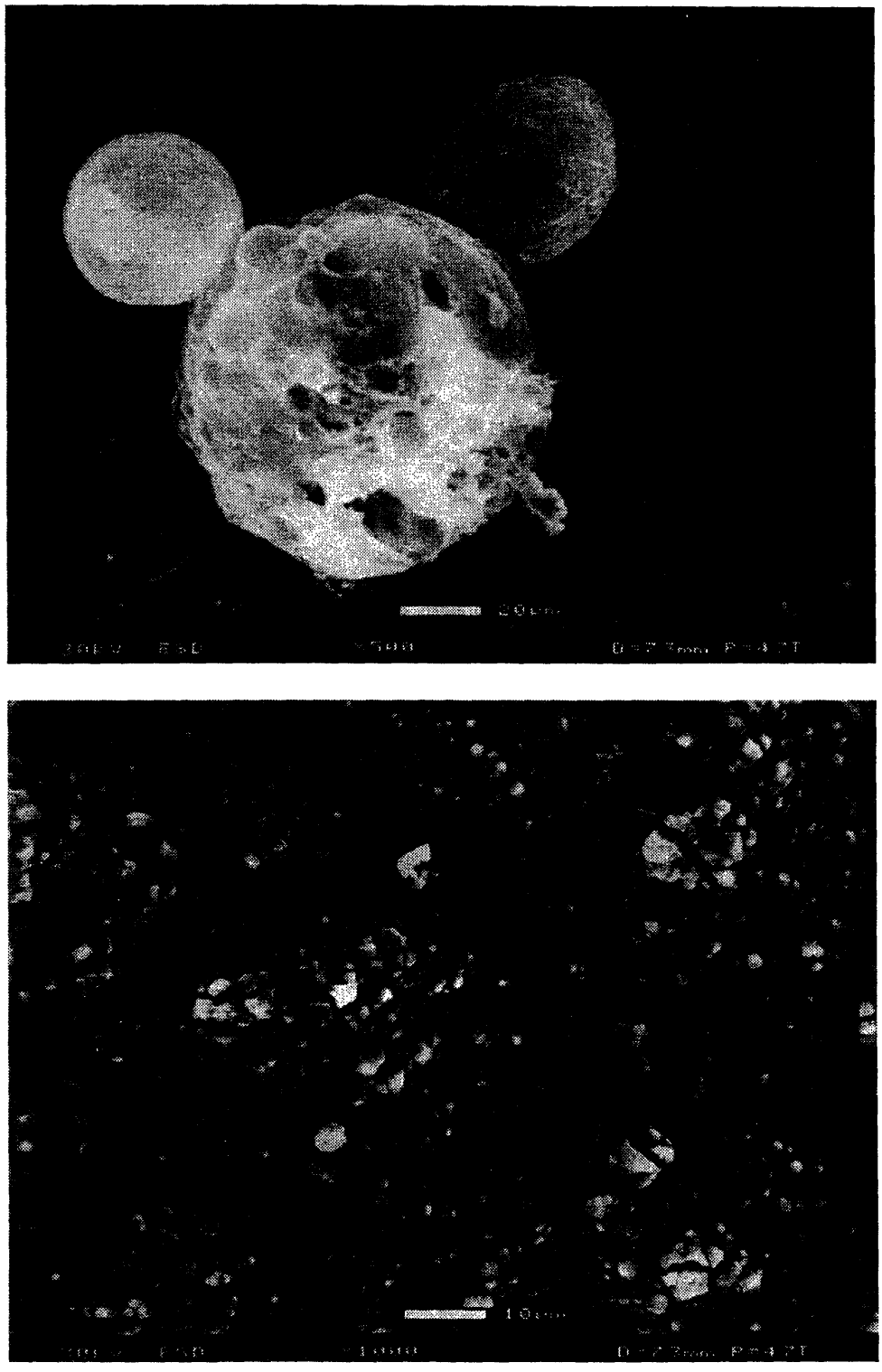

Figure 4.15 ESEM micrographs of Nb exposed to $P_{O_2} = 10^{-20.6}$ atm and $P_{S_2} = 10^{-7.6}$ atm at 800°C for 20 hours: (a) Nb_2O_5 particles on NbO_2 and (b) NbO_2 scale.

4.3.2 Results at 900°C

The performance of the CrNb relative to that of Cr and Nb, in O_2 and S_2 pressures of 10^{-18} atm and 10^{-8} atm respectively (gas composition B) can be seen in Figure 4.16. GAXRD revealed a chromia scale on the CrNb with no sulfides indicated. This brought the behavior of CrNb very close to that of pure Cr, which exhibited chromia formation at a parabolic rate of $2X10^{-12}$ g^2/cm^4 sec. A cross section of the CrNb scale showed a distinct outer layer of chromia with an inner layer that gave a mix of Cr, Nb and sulfur XEDS signals. This may be a mix of sulfides, since the niobium elemental map was not continuous in the inner scale region (Figure 4.17). The Nb had an oxidation rate much higher than that of CrNb or Cr. The scale consisted of NbO_2 with some small amounts of Nb_2O_5 (Figure 4.18). The niobium scale after oxidation/sulfidation was difficult to characterize, owing to the overlap of the niobium oxide peaks. The peaks were consistent with Nb_2O_5, with some lower-angle peaks missing. The JCPDS card for NbO_2 provided a perfect match to the data with no missing or extra peaks. The presence of Nb_2O_5 is assumed, despite the imperfect match, because of the observation of a powdery, white scale concentrated at the edges. Nb_2O_5 is white and porous, while NbO_2 is black.

Gas Composition C (-18, -5.6) 900°C This composition (-18, -5.6) lies on the sulfide side of the kinetic boundary for pure Cr and yields large weight gains and sulfide formation. CrNb reacted in this gas yielded chromia and probable $CrS_{1.17}$ according to GAXRD. In the XEDS maps, sulfur is observed uniformly interspersed in the middle of the scale (Figure 4.19).

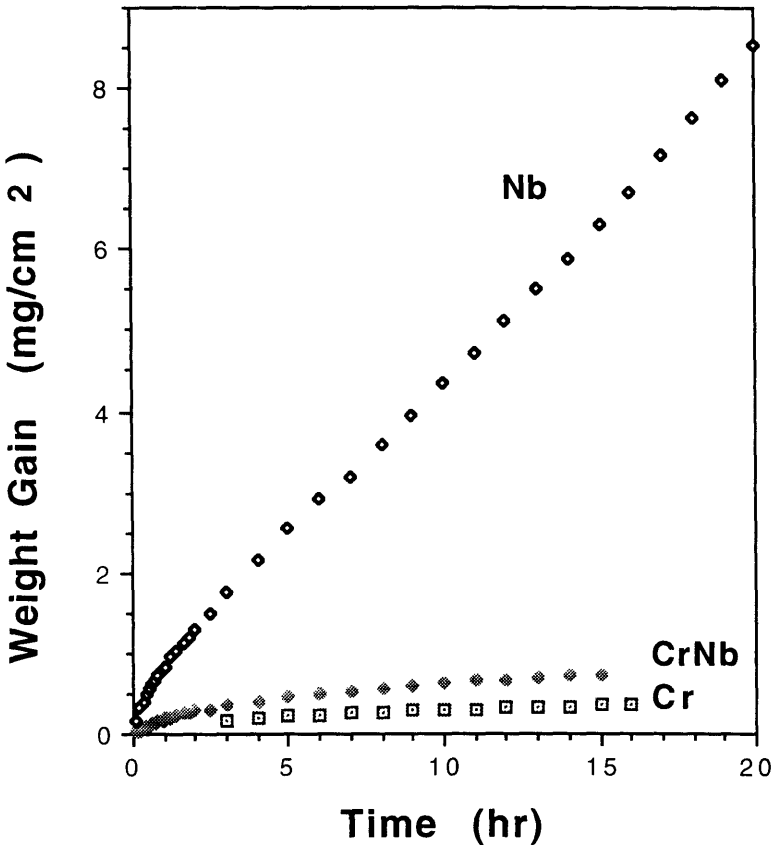

Figure 4.16 Weight gain versus time for Cr, Nb and CrNb exposed to $P_{O_2} = 10^{-18}$ atm and $P_{S_2} = 10^{-8}$ atm at 900°C for 20 hours.

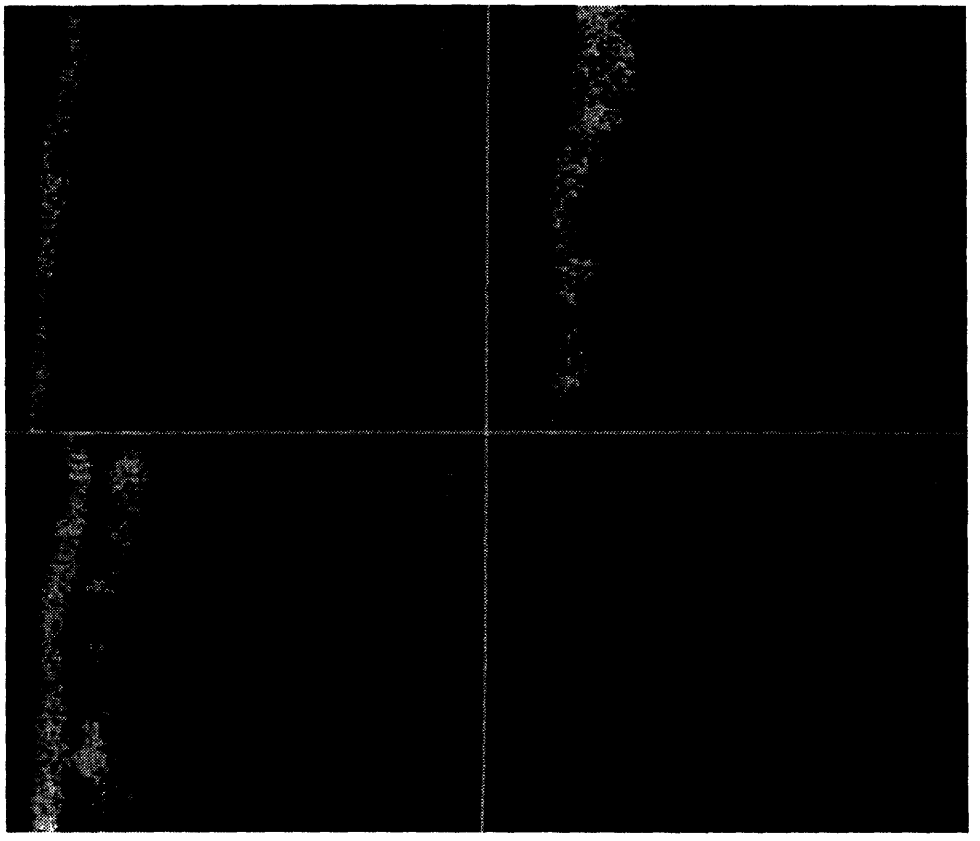

Figure 4.17 ESEM binary XEDS maps of CrNb exposed to $P_{O_2} = 10^{-18}$ atm and $P_{S_2} = 10^{-8}$ atm at 900°C for 20 hours.

Figure 4.18 ESEM micrograph of Nb exposed to $P_{O2} = 10^{-18}$ atm and $P_{S2} = 10^{-8}$ atm at 900°C for 20 hours.

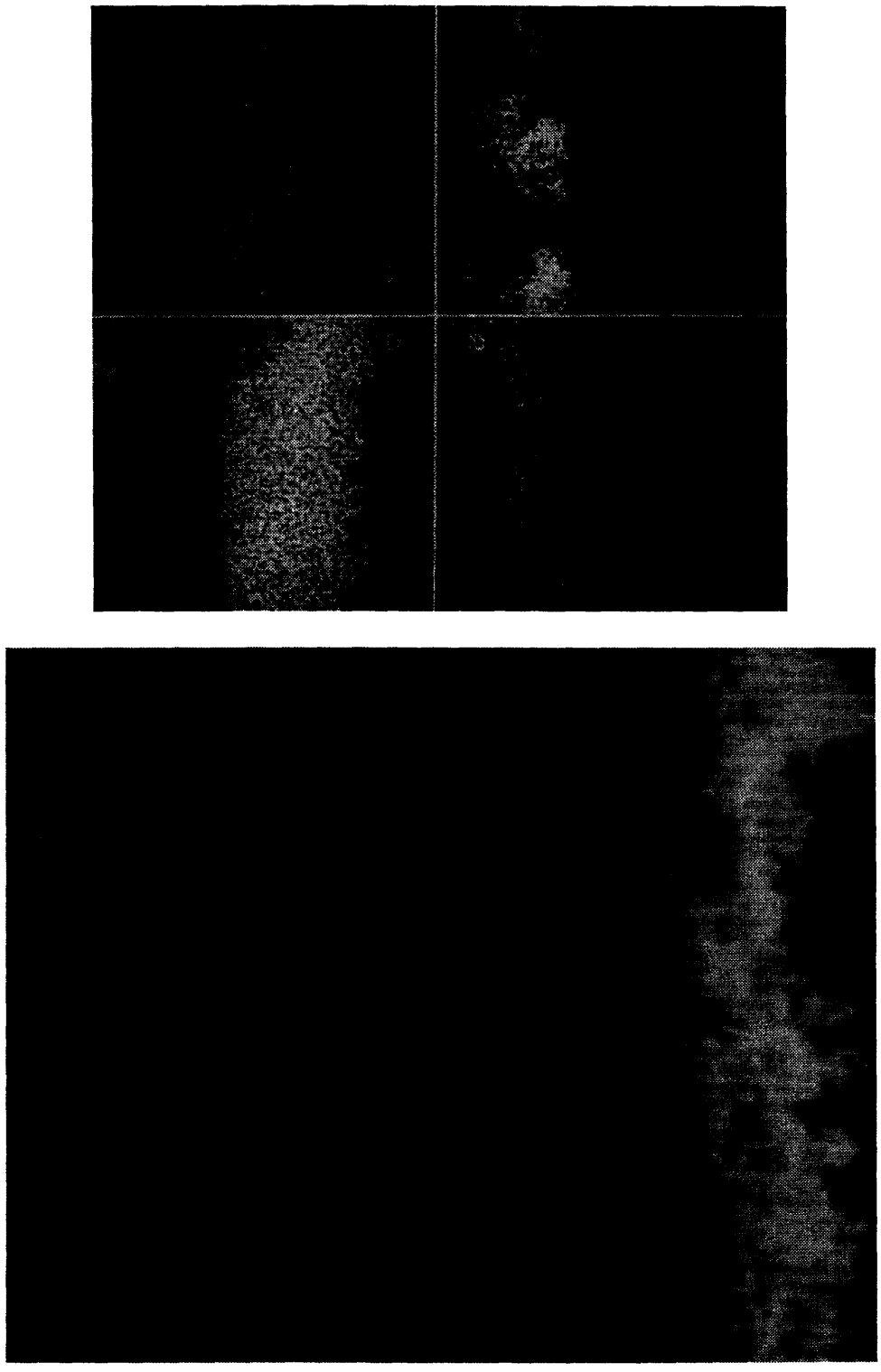

Figure 4.19 ESEM binary XEDS maps and corresponding micrograph of CrNb exposed to $P_{O_2} = 10^{-18}$ atm and $P_{S_2} = 10^{-5.6}$ atm at 900°C for 3 hours.

Gas Composition F (-19.0, -6.5) 900°C An additional oxidation/sulfidation gas composition with significantly higher sulfur pressure ($10^{-6.5}$ atm) and slightly lower oxygen partial pressure (10^{-19} atm) than gas composition B was used at 900°C. The thermogravimetric behavior of the alloys is shown in Figure 4.20. The NbCr grew to a scale thickness of less than 5 μm, while CrNb behaved with nearly identical behavior to Cr. The kinetic rate for the NbCr alloy was more than 2 times higher than that for CrNb. The CrNb formed a continuous Nb sulfide inner layer in addition to a considerable chromia outer layer. In the case of NbCr, the inner sulfide region is larger and less sharp. In both cases the outer oxide scale had detectable niobium signal, indicating a doping of the chromia scale by niobium. The corrosion rate for the pure Cr in this gas was about three times faster than for a pure Cr sample run on the chromia side of the kinetic boundary. The cross section shows significant sulfur in the scale and particularly at the metal/scale interface. The FeCrNb alloy displayed linear catastrophic corrosion kinetics, gaining weight faster than Nb.

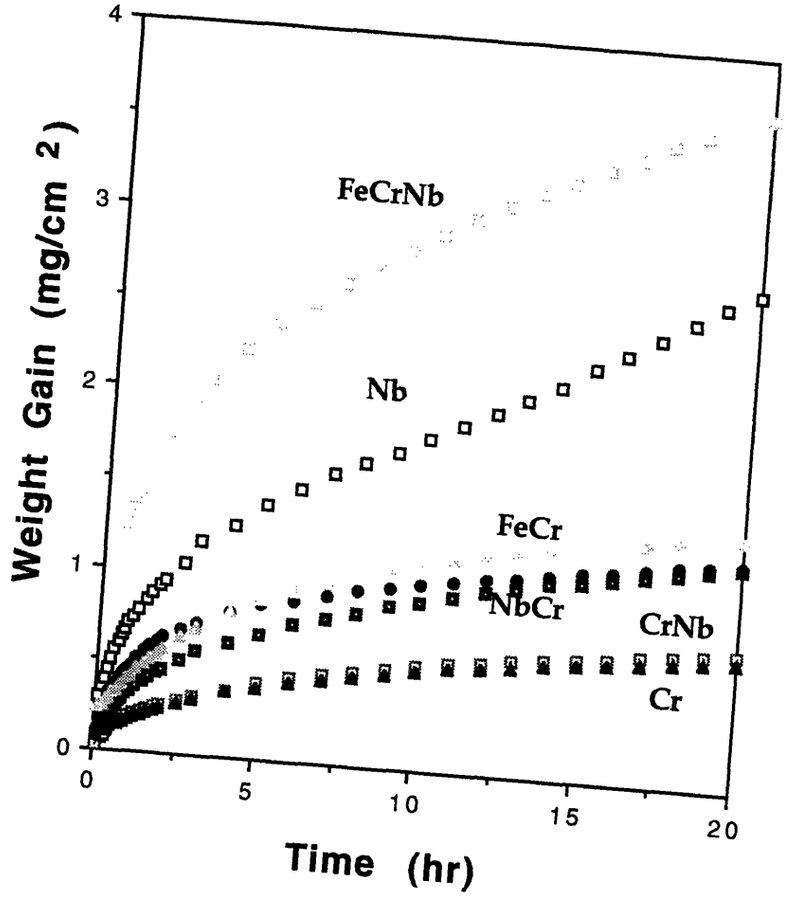

Figure 4.20 Weight gain versus time for Cr, Nb, FeCr, FeCrNb, NbCr and CrNb exposed to $P_{O_2} = 10^{-19}$ atm and $P_{S_2} = 10^{-6.5}$ atm at 900°C for 20 hours.

Overall, the weight gains of all alloys were considerably less than those obtained by Douglass and coworkers (He 1992; Kai 1992; Shing 1992) on a range of other binary Nb alloys. The CrNb alloy displayed a scale growth rate nearly identical to that of pure Cr. GAXRD determined the scale on the alloy to be essentially chromia with possibly NbS_2. X-ray maps of cross sections indicate a chromium oxide scale with a niobium sulfide layer beneath (Figure 4.21). For pure Cr, cross sections show oxide and sulfide layers as well, though the sulfur layer is less prominent and X-ray diffraction detected only a chromia scale (Figure 4.22 and 4.23). Gas composition F lies close to the kinetic boundary for Cr. For the NbCr alloy, duplex oxide/sulfide layers also exist but were much less defined, and the scale is much thicker (Figure 4.24). It was also difficult to confirm whether the niobium sulfide layer was continuous, though it appeared so. The inner layer could result from Cr depletion of the NbCr alloy as Cr diffuses out.

Chromia X-ray peaks from FeCr scales were weak, despite the similarity of its growth kinetics to those of NbCr scales; iron sulfides were detected as well. The scale on pure Nb was a mixture of oxides and sulfides. The scale on FeCrNb alloy was a mix of $CrNbO_4$/$FeNbO_4$ and a little chromia, similar to the product in pure oxidation conditions.

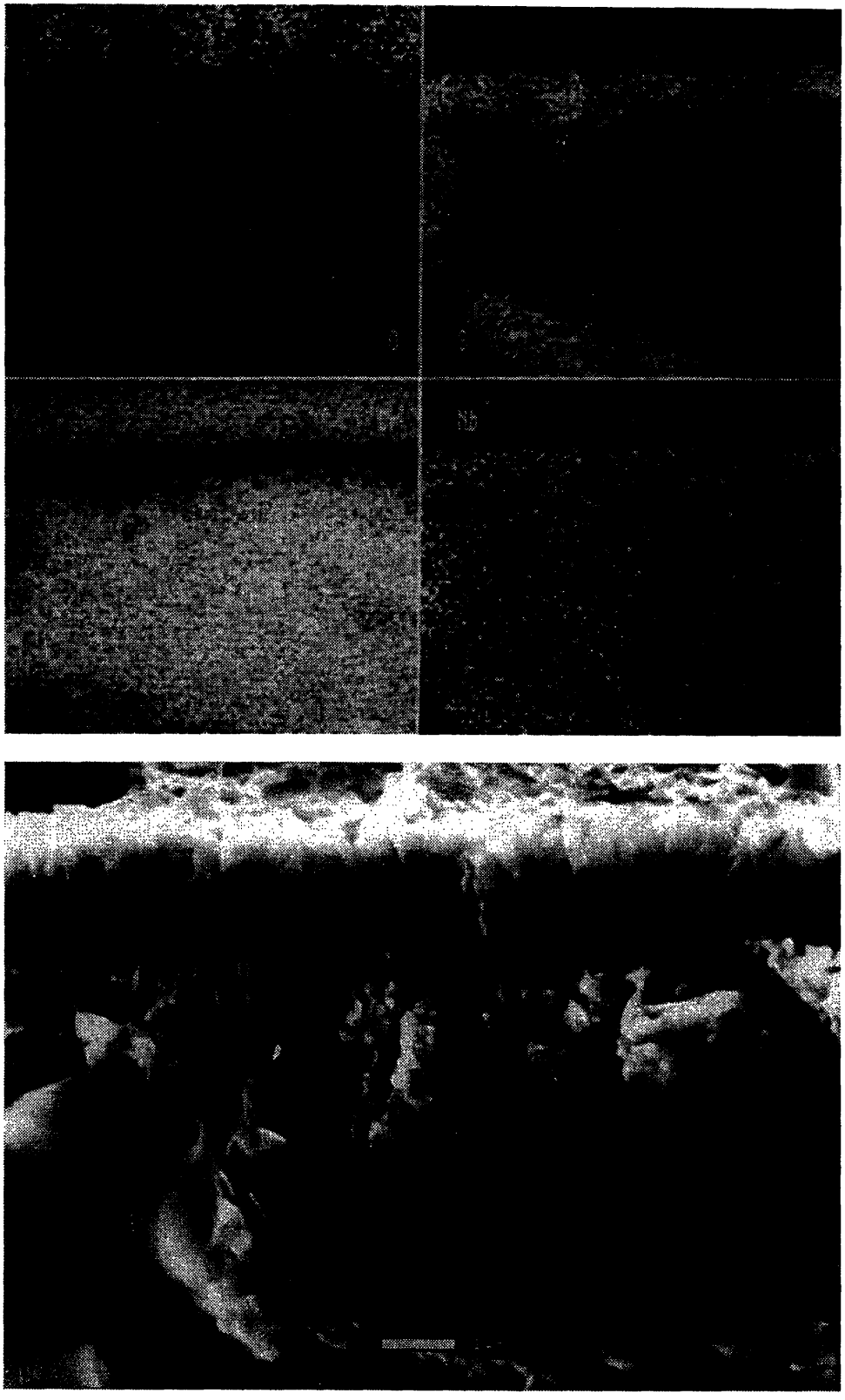

Figure 4.21 ESEM binary XEDS maps and corresponding micrograph of CrNb fracture cross section exposed to $P_{O_2} = 10^{-19}$ atm and $P_{S_2} = 10^{-6.5}$ atm at 900°C for 20 hours.

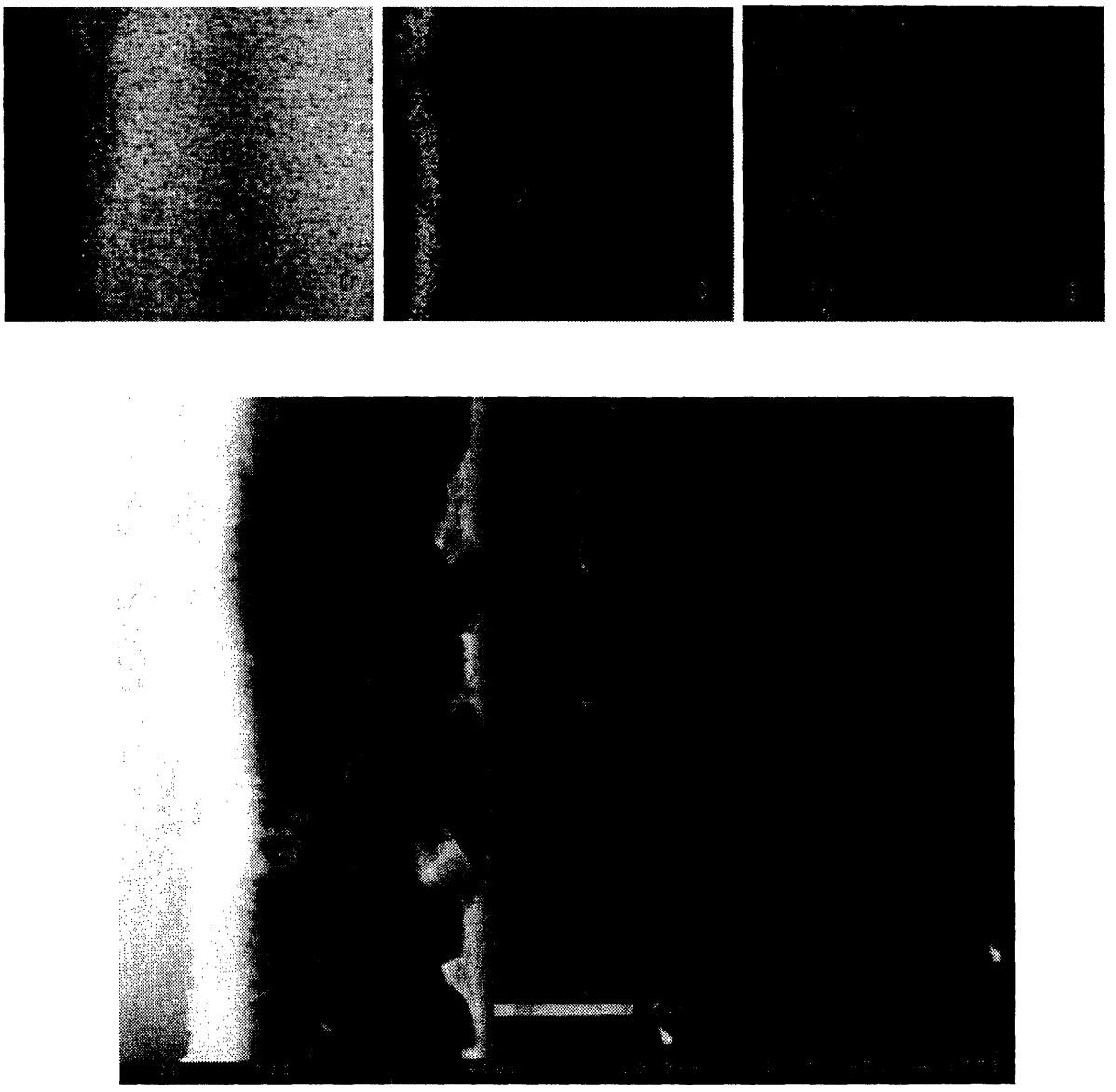

Figure 4.22 ESEM binary XEDS maps and corresponding micrograph of Cr fracture cross section exposed to $P_{O_2} = 10^{-19}$ atm and $P_{S_2} = 10^{-6.5}$ atm at 900°C for 20 hours.

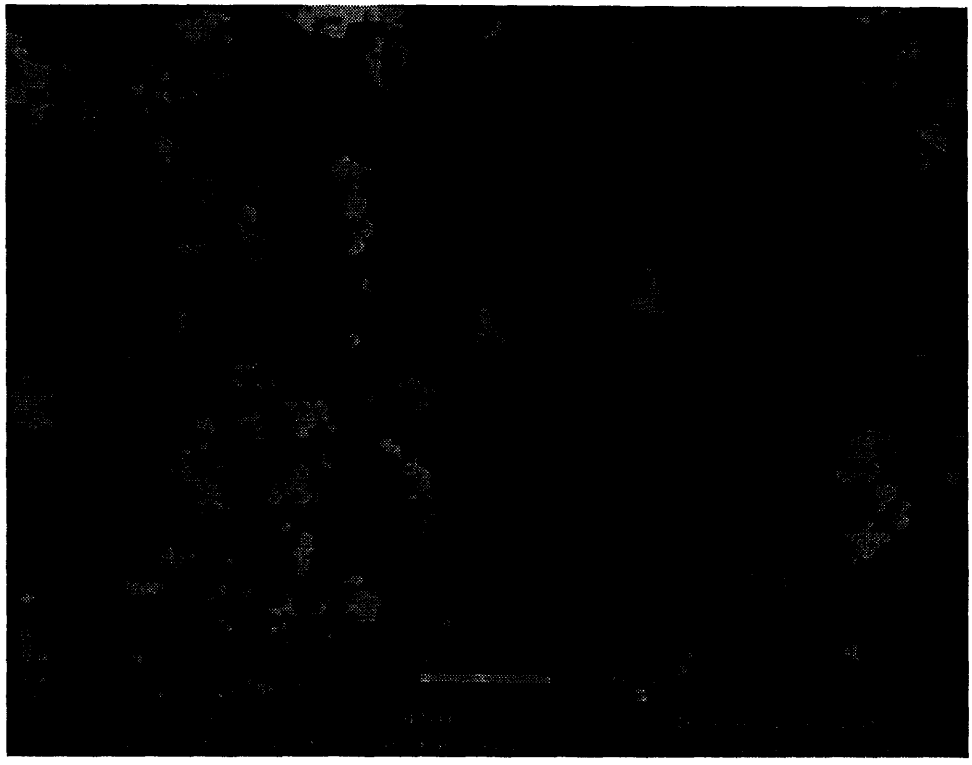

Figure 4.23 ESEM micrograph of Cr exposed to $P_{O_2} = 10^{-19}$ atm and $P_{S_2} = 10^{-6.5}$ atm at 900°C for 20 hours.

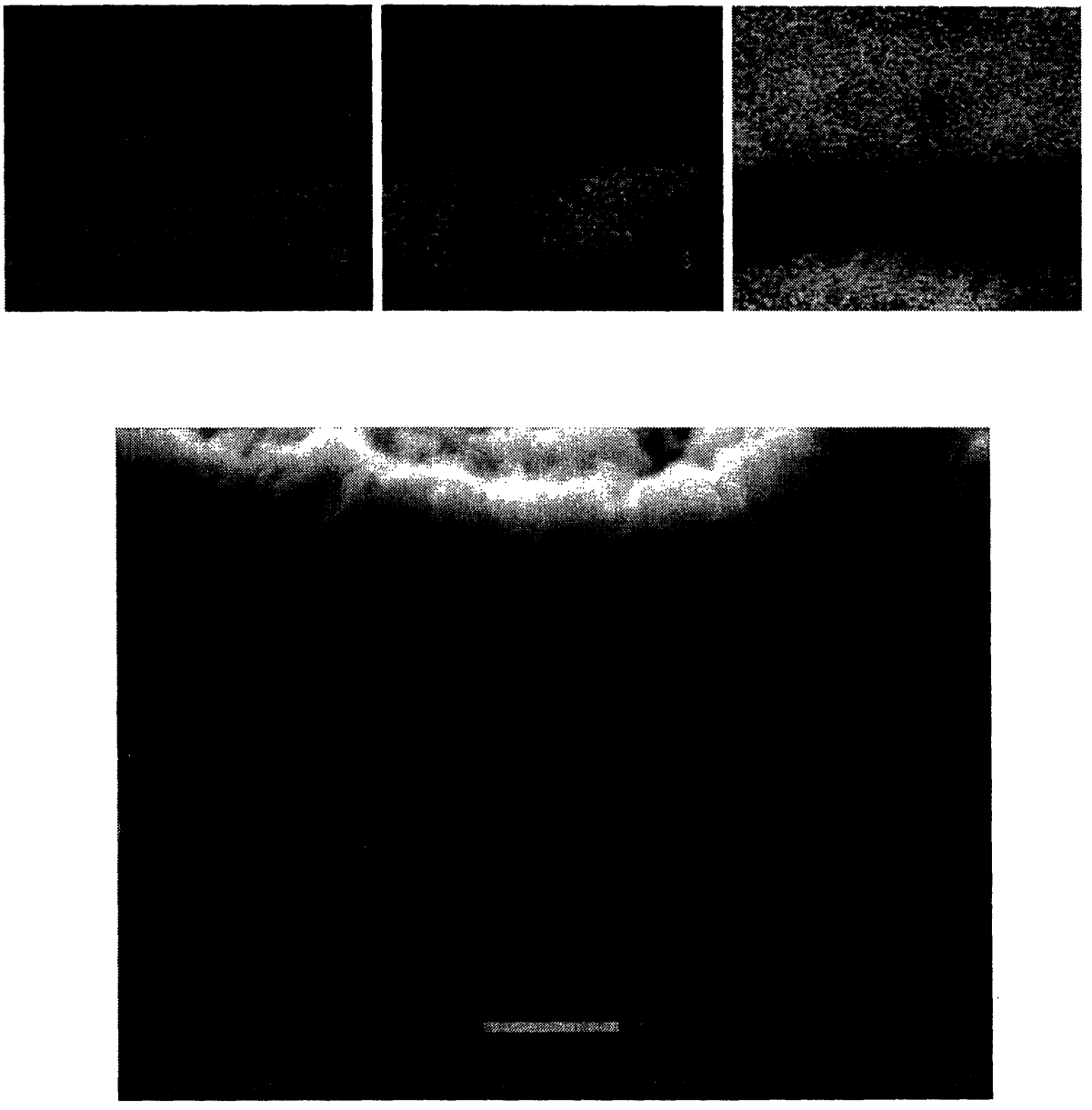

Figure 4.24 ESEM binary XEDS maps and corresponding micrograph of NbCr fracture cross section exposed to $P_{O_2} = 10^{-19}$ atm and $P_{S_2} = 10^{-6.5}$ atm at 900°C for 20 hours.

Chapter 5

Discussion

5.1 Oxidation/Sulfidation in SO_2

The condensation of sulfuric acid on the hangdown wire and the resulting irreproducibility rendered much of the TGA data for corrosion in SO_2 meaningless. It must also be taken into account that the oxygen and sulfur partial pressures that arise from using pure sulfur dioxide are not representative of those seen in energy systems and therefore may not lead to useful prediction of the behavior of alloys in coal gasification conditions. The higher oxygen partial pressure permits the formation of chromia, as seen on CrNb; the high oxygen pressure also results in catastrophic Nb oxidation. Some difficulty occurs in accurately determining P_{O2} and $P_{S2,}$ since these pressures are dependent on the oxygen impurity level, both in the cylinder and from residual amounts in the furnace system.

Another consideration in the use of SO_2 is the corrosion of the furnace system from the liquid and gaseous acid. The glassware and quartz hook were etched, and the Pt hangdown wire was corroded. Stainless steel fittings at the bottom of the furnace, where the condensed acid accumulated, acquired holes in the course of experiments,

compromising the isolation and control of furnace environment and therefore the precision of the calculated gas compositions. The acid fumes are possibly damaging to the microbalance and the alumina furnace tubes. Utilizing the H_2-H_2O-H_2S mixtures eliminated these problems and afforded flexibility in selecting gas compositions.

5.2 Sulfidation in H_2-H_2S Mixtures

Gas Composition S1. The formation of NbS_2 is one anticipated mechanism for scale protectiveness in the Cr-Nb system. In S1 at 800°C, the scale on the pure Nb was $Nb_{(1-x)}S$ not NbS_2. The Nb deficiency scale is expected to aid diffusion of species through the scale and accelerate scale growth. The inability of pure Nb to form a protective scale at low P_{S_2} would lead one to the conclusion that the binary alloy would not be able to form NbS_2 due to the lowered activity of Nb in the alloy. The niobium-rich region detected on the CrNb may be a niobium sulfide or simply adjacent to a localized alloy depletion. At the same pressure (S1) at 900°C, NbS_2 as well as Nb_3S_4 were detected on the Nb samples. Of the Cr-Nb alloys, only the scale on NbCr contained NbS_2; the scale on CrNb contained the niobium-deficient sulfide, which may indicate that there is insufficient Nb activity for NbS_2 formation.

S1/S2 NbCr. An interesting experiment was conducted to explore the effect of sulfur pressure on the corrosion resistance and scale adherence of the NbCr alloy. The alloy was reacted with a gas of composition S1, which spalled. After exposure of 2 hours, the composition of the gas was switched *in situ* to the higher S2 pressure while maintaining the sample at temperature. The reaction rate changed after the gas composition was altered and overall the sample exhibited an adherent scale like that of other samples exposed to S2 only , with no spallation such as observed for samples exposed to S1. Evidently, a minimal, critical sulfur pressure is required for the formation of a Nb sulfide that slows the corrosion as well as aids in the formation of a protective, adherent scale.

Sulfur partial pressure was shown to have no significant effect on the kinetic rates for NbCr at 900°C for those gas compositions studied. The rates were within one order of magnitude of each other, independent of the pressure. One notable difference is the lack of spallation at the higher sulfur pressures. The curves showed parabolic behavior with different regimes, arguably different rates for the formation of niobium sulfides or chromium sulfides. Since the kinetics were not appreciably different at the different pressures, it was at first presumed that the scales might be similar, but there is clearly a wide disparity in the X-ray diffraction scans indicating the formation of different sulfides. From work at 800°C, one could speculate that insufficient sulfur was available for the formation of the stable NbS_2 scale. Lower pressures may allow nonstoichiometric sulfide formation (e.g., $Nb_{1-x}S$) as found in S1 at 800°C on pure Nb.

Also, CrNb also exhibited a kinetic rate seemingly independent of temperature for the gas S1 at 800°C and 900°C. An insufficient range of temperatures was investigated to determine the exact nature of the dependence.

5.3 Oxidation/Sulfidation in H_2-H_2O-H_2S Mixtures

Gas Composition A (-20.6, -7.6) 800°C. Gas mixture A has a low oxygen pressure and a rather aggressive sulfur pressure. The mix of oxide and sulfides in the Cr scale suggested an environment near the kinetic boundary (LaBranche 1987) The macroscopic surface roughness, blades and large needles was often observed in chromium sulfides scales on Cr-bearing substrates. The niobium scale, which was the slowest growing scale of the series, consisted of NbO_2. This was surprising, since the small weight gain and dark scale suggested NbS_2. However, pure sulfidation studied at even higher sulfur pressures than those in mixture A did not form NbS_2, so the sulfur pressure was not high enough in atmosphere A to form a protective NbS_2 scale on Nb. From this result, one

would not expect that diluting the Nb with Cr would produce an increased likelihood of NbS_2 formation under the same conditions. This high sulfur requirement could be used advantageously in lower-grade coals which contain higher amounts of sulfur. The micrograph (Figure 4.15) showed cracks on the top of small hills in the Nb scale, suggesting cracking at temperature rather than during cool down. In general, this gas series was not too illustrative of gas conditions seen in real applications nor of particularly protective behavior.

Gas Composition B (-18.0, -8.0) 900°C. These conditions are typical to those experienced in coal gasification processes. The temperature of 900°C was used by LaBranche (1985) for pure Cr and by Zhou (1993) with CrNb, so comparisons could be made readily to their results. The kinetic boundary for pure Cr was determined at 900°C (LaBranche 1987) and gas composition B lies within the chromia stability region. The kinetic rate constant was approximately ten times faster than that for pure Cr. No sulfides were detected with GAXRD but XEDS indicated a layer containing Cr, Nb and sulfur beneath the chromia. Unfortunately, the ESEM does not have the spatial and compositional resolution that TEM can offer, so more precise determination of the scale and individual components was not possible without recourse to TEM.

Gas Composition C (-18.0, -5.6) 900°C. CrNb was exposed to gas mixture C for 2 hours to evaluate transition effects and to compare the behavior of CrNb to that of Cr at compositions beyond the kinetic boundary in the sulfide regime. This gas composition lies on the sulfide side of the kinetic boundary for pure chromium, so a sulfide of chromium therefore is expected to be stable kinetically. The composition was used to see what effect, if any, Nb had on the corrosion behavior. CrNb cross sections revealed the presence of both oxygen and sulfur in the scale. Niobium was enriched below the scale

(from the outward diffusion of Cr to form this mixed oxide/sulfide scale). Also sulfur was significantly enriched below the scale, presumable diffusing in and internally sulfidizing the niobium enrichment there. However, this niobium/sulfide reaction product is not continuous and gave no indication of NbS_2 formation; therefore it would not expected to be protective over longer times. This is one of the few cases where internal sulfidation was observed in these experiments.

Gas Composition F (-19.0, -6.5) 900°C. This composition contained significantly higher sulfur pressure and slightly lower oxygen partial pressure compared to gas composition B. Higher sulfur was chosen to enable the formation of a protective niobium product without proscribing chromia formation. It was surprising to find that, while NbCr proved very resistant (growing to a scale thickness less than 5 μm), the CrNb alloy behaved nearly identically to the pure Cr. The corrosion rate of the NbCr alloy was over two times larger than that of CrNb. At this sulfur pressure, it was hoped that Nb would sulfidize without appreciable chromium sulfide formation, but it appears that the CrNb formed a continuous Nb sulfide inner layer in addition to a considerable chromia outer layer. In the case of NbCr, the inner sulfide region is larger and less dense, perhaps indicating that only sulfur is diffusing in and reacting in the Cr depleted region at the scale/alloy interface. The discontinuous scale accounts for the inability to keep the kinetic rate down in the case of NbCr. In both CrNb and NbCr, the outer oxide scale had a significant niobium content, indicating a doping of the chromia scale by niobium. The rate for the pure Cr in this gas was about three times faster than for a pure Cr sample run at just into the chromia side of the kinetic boundary conditions. The cross section shows significant sulfur in the scale and particularly at the metal/scale interface. The FeCrNb alloy had catastrophic corrosion behavior, gaining weight faster than even the pure Nb.

5.4 Comparison of CrNb to NbCr

NbCr alloy, with higher Nb content, was manufactured in the hope of forming protective niobium product scales. Neither glancing angle x-ray diffraction nor SEM studies showed significant niobium sulfide content in the CrNb scales.

Not only a higher Nb content seemed necessary to generate niobium reaction products, but also a minimal sulfur pressure was also needed to activate the formation of niobium sulfide. This agreed well with Zhou (1993) observation of a continuous niobium sulfide inner layer when reacted with pure sulfur vapor at a partial pressure of 0.76 atm. It appears that the gas composition A was below the minimal sulfur pressure required to form niobium sulfide at this temperature. Thermodynamically, using the data from Larson (1967), a pressure exceeding $P_{S_2} = 6.9 \times 10^{-13}$ atm should be in equilibrium with solid NbS_2 at 900°C. The sulfur pressure used exceeded this equilibrium value; the presence of oxygen had the effect requiring increased sulfur to produce the protective sulfide.

5.5 Comparison of Cr-Nb alloys to FeCrNb

In all cases, the behavior of the FeCrNb alloy was worse than the Cr-Nb alloys and the pure Nb or Cr constituents. It was also noted that the specimen appeared to be porous after polishing and this lack of complete densification may have affected the kinetics observed. However, even the preliminary pure sulfidation and the mixed oxidation/sulfidation in gas composition F (rather aggressive sulfur with low oxygen partial pressure) indicated that the usefulness of this alloy is questionable, so further extensive studies were abandoned.

Fracture cross sections of FeCrNb revealed a thick scale (more than 20 μm) with porosity and a convoluted scale/metal interface that made thickness determination difficult. The

X-ray maps showed a complex scale (not duplex with any particular oxide or sulfide); naturally, a continuous layer of chromia or niobium sulfide or both would be desirable. From the element maps, the scale was a rather complicated mix of oxysulfides for any of the constituent elements iron, chromium or niobium. The porosity also suggests that this material will not be protective in the environments being considered. The absence of a distinctive scale phase is the probably cause for its poor corrosion resistance.

Also, as so far as workability is concerned, it should also be noted that no great benefit accrued. Slicing this alloy with the usual low speed diamond saw took 20 hours (the boron nitride blade reduced it to about 5 hr), compared to a typical superalloy slicing time of several hours. Also, the hole for hanging the specimen required sandblasting, since the tungsten carbide blade made no noticeable penetration. By way of comparison, CrNb and NbCr both require sandblasting and are extremely brittle; samples could be broken with little force or by dropping. The FeCrNb showed no such brittleness. The Cr was relatively hard but could be drilled with regular drill bits. The niobium was very ductile and easy to polish, cut and drill. From these observations, one could surmise that only modest workability was gained at the expense of a large loss in corrosion resistance.

GAXRD revealed CrNb intermetallic peaks on the FeCrNb. This may indicate a heterogeneity in phase distribution which could lead to preferential attack, detrimental to the corrosion behavior of the alloys. The attempt to incorporate Cr and Nb into a base material (at least with Fe) did not produce satisfactory results. The most probable way to use a Cr-Nb alloy to impart simultaneous resistance may be as a coating, using techniques similar to those used in the aerospace industry for deposition of nickel aluminide coatings.

Chapter 6

6.0 Conclusions

- There exist simultaneous oxidation/sulfidation conditions where CrNb and NbCr behave similarly to simple Cr oxidation or Nb sulfidation.
- The complexity of a binary system in mixed oxidants greatly limits generalization about corrosion behavior. A case-by-case study may be necessary to determine the appropriate Cr-Nb alloy composition for a specific corrosive environment.
- CrNb behaves similarly to pure Cr with respect to its kinetic boundary.
- Minimum sulfur pressures and a minimum Nb content may be necessary to form NbS_2 preferentially to other possible niobium sulfides.
- NbO_2 as well as NbS_2 may contribute to scale protectiveness. NbO_2 is formed at nonequilibrium conditions according to available thermodynamic data.

Chapter 7

Future Work

Prior to this work, the Cr-Nb binary system was completely unstudied in mixed oxidants. The complexity of a binary system and mixed oxidation/sulfidation allow for more exploration Since the Cr_2Nb intermetallic shows promise for use in simultaneous oxidation/sulfidation environments, the experiments in this work could be augmented by:

- Analytical microscopy, especially TEM on both parallel and transverse sections, would be enlightening. This would be novel work, since only chromia scales grown in small sulfur partial pressures have been previously studied (LaBranche 1985). The adverse effect of sulfur on scale adhesion makes TEM investigation a particularly challenging avenue to pursue. The analysis of TEM samples from duplex scales would yield extremely valuable information into the scale compositions and growth mechanisms. The resolution of conventional SEM or microprobes does not allow for precise characterization of scales. In thin protective scales, of interest in corrosion applications, the segregation of different components is best resolved using transmission electron microscopy.

- Alternative TEM specimen preparation methods are available, especially for producing transverse sections of the thicker or complex scales. One potential method, focused ion beam etching, has potential for producing large uniformly thin sections in a selected area of interest on the sample.

- The use of EDM for TEM sample preparation is another such possibility The amount of damage introduced is an area of concern. Additionally, the scale must be sufficiently conductive enough to be sensed by the EDM.

- More thorough investigation into the mechanisms of why certain compositions were more protective in specific conditions is warranted. Several results were surprising, and an in-depth look, with isotopic tracers or other analytical techniques, could pinpoint trends in corrosion behavior in this system.

- The exploration of many other gas compositions is certainly indicated. Although several representative compositions were investigated in this study, specific gas compositions relevant to actual applications can be studied.

- A study of the relation between kinetic rate and sulfur or oxygen partial pressure could be made to obtain activation energies . A comparison with activation energies for the pure components could provide insight into the corrosion mechanisms.

- The construction of a kinetic boundary for either CrNb or NbCr and the comparison to that for pure Cr would prove valuable, particularly for application to real systems. A comparison could also be made to the Nb stability diagram; however,

incomplete or conflicting thermodynamic data make the Nb stability diagram more questionable (Larson 1967 and Worrell 1964).

- The use of a reactive agent, either by alloy addition or by ion implantation, could improve alloy performance particularly in the formation of chromia. This technique holds the potential of greatly improving the corrosion resistance and has the advantage of being well studied and established on chromia formers. Ion implantation would be the easiest to implement at this stage without requiring the manufacture of new materials. Ion implantation has also been shown to be more effective in aiding the formation of protective scales in chromia formers compared to alumina formers.

- A feasibility study of this material could assess the practical utility for application in fossil fuel systems. As a binary alloy, the cost of Cr and Nb is prohibitive for use as a structural material. Coating and powder metallurgy techniques may be necessary to bring the corrosion benefits of the alloy to actual use applications. Due to the significant portion of intermetallic compound in the alloys, working with the Cr-Nb system is not simple. The brittleness of Cr_2Nb exceeded that of many commonly used intermetallics such as NiAl, Ni_3Al, Ti_3Al, etc.

References

M.F. Chen, D.L. Douglass, and F. Gesmundo, (1989) "High'Temperature Sulfidation Behavior of Ni-Nb Alloys", Oxid. Met., V. 31 p. 237.

D.J. Derry and D.G. Lees (1976) "The Oxidation Behavoiur of a Niobium-Chromium-Nickel Alloy" Corr. Science, v. 16, p 219.

B. Gleeson, D.L. Douglass, and F. Gesmundo (1989) "Effect of Nb on the High-Temperature Sulfidation Behavior of Cobalt" Oxid. Met., V. 31 p. 209.

Y.-R. He, D. L. Douglass, and F. Gesmundo, (1992) "The Corrosion Behavior of Ni-Nb Alloys in a Mixed Gas of H_2-H_2O-H_2S", Oxid. Met., v. 37 p. 217.

W. Kai, D. L. Douglass, and F. Gesmundo, (1992) "The High-Temperature Corrosion of Fe-Nb Alloys in a $H_2/H_2O/H_2S$ Gas Mixture", Oxid. Met. v. 37 p. 189.

Y.K Kim (1988) "Mechanisms of the Oxidation/Sulfidation of Chromium and Chromium-Bearing Alloys in H_2-H_2O-H_2S Gas Mixtures", MIT Ph.D. Thesis.

P. Kofstad (1988) High Temperature Corrosion, Elsevier Applied Science, London and New York.

M. LaBranche, A. Garratt-Reed, and G. J. Yurek, (1983) "Early Stages of the Oxidation of Chromium in H_2-H_2O-H_2S Gas Mixtures", J. Electrochem. Soc., v. 130, #12, p. 2405.

M.H. LaBranche, (1985) "Part I: The Oxidation of Chromium at Low and High Oxygen Partial Pressures Part II: The Oxidation/Sulfidation of Chromium in H2-H2O-H2S Mixtures", MIT Ph.D. Thesis.

M. H. LaBranche and G. J. Yurek, (1987) "Kinetics and Mechanisms of the Oxidation of Chromium in H_2-H_2O-H_2S Gas Mixtures", Oxid. Met. v. 28 p. 73.

H. R. Larson and J. F. Elliot, (1967) "The Standard Free Energy of Formation of Certain Sulfides of Some Transition Elements and Zinc", Trans. Met. Soc. AIME, v. 239, p. 1713.

C. C. Shing, D. L. Douglass, and F. Gesmundo, (1992) "The High-Temperature Corrosion Behavior of Co-Nb Alloys in Mixed-Gas Atmospheres", Oxid. Met. v. 37 p. 167.

B. Soumendra, (1989) "Mechanisms of Oxidation of Crystalline Rapidly-Solidified Alloys", MIT Ph.D. Thesis.

K.N. Strafford and J.R. Bird, (1979) "The kinetics of sulphidation of niobium", J. Less Common Met., v. 68, p 223.

K. Tatsuki, M. Wakihara, and M. Taniguchi, (1979) "Phase Relations in the Nb-S System at High Temperatures", J. Less Common Met., v. 68 p. 183.

P.F. Tortorelli and J.H. DeVan, (1992) "The Effect of Nb on Scales Grown on Cr-Nb Alloys", Electrochemical Society Extended Abstracts, V. 92-3, P. 231.

G. Wang, R. Carter, and D. L. Douglass, (1989) "High Temperature Sulfidation of Fe-Nb Alloys", Oxid. Met., v. 32 p. 273

W. L. Worrell, (1964) "The Free Energy of Formation of Niobium Dioxide between 1100 and 1700°K" J. Phys. Chem., v. 68, # 4, p. 952.

C. Zhou, (1991) "Growth, Structures, and Properties of Cr_2O_3 and NbS Corrosion Scales", MIT PhD Thesis.

C. X. Zhou and L. W. Hobbs, in *Proc. 3rd International Symp. on High Temp. Corrosion and Protection of Materials*, ed. R. Streiff, J. Stringer, R. C. Krutenat and M. Caillet, J. Physique IV **3** (Colloque C9) 339 (1993).